National Library of Canada
Canadian Theses Service
Ottawa, Canada
K1A 0N4

Bibliothèque nationale du Canada
Service des thèses canadiennes

NOTICE

The quality of this microform is heavily dependent upon the quality of the original thesis submitted for microfilming. Every effort has been made to ensure the highest quality of reproduction possible.

If pages are missing, contact the university which granted the degree.

Some pages may have indistinct print especially if the original pages were typed with a poor typewriter ribbon or if the university sent us an inferior photocopy.

Previously copyrighted materials (journal articles, published tests, etc.) are not filmed.

Reproduction in full or in part of this microform is governed by the Canadian Copyright Act, R.S.C. 1970, c. C-30.

AVIS

La qualité de cette microforme dépend grandement de la qualité de la thèse soumise au microfilmage. Nous avons tout fait pour assurer une qualité supérieure de reproduction.

S'il manque des pages, veuillez communiquer avec l'université qui a conféré le grade.

La qualité d'impression de certaines pages peut laisser à désirer, surtout si les pages originales ont été dactylographiées à l'aide d'un ruban usé ou si l'université nous a fait parvenir une photocopie de qualité inférieure.

Les documents qui font déjà l'objet d'un droit d'auteur (articles de revue, tests publiés, etc.) ne sont pas microfilmés.

La reproduction, même partielle, de cette microforme est soumise à la Loi canadienne sur le droit d'auteur, SRC 1970, c. C-30.

NL-339 (r. 88/04)

Canada

THE UNIVERSITY OF ALBERTA

THE MEASUREMENT OF ELECTROGASTROGRAM

by

© Dalu PENG

A THESIS

SUBMITTED TO THE FACULTY OF GRADUATE STUDIES AND RESEARCH

IN PARTIAL FULFILMENT OF THE REQUIREMENTS

FOR THE DEGREE OF MASTER OF SCIENCE

DEPARTMENT OF ELECTRICAL ENGINEERING

EDMONTON, ALBERTA

FALL, 1988

Permission has been granted to the National Library of Canada to microfilm this thesis and to lend or sell copies of the film.

The author (copyright owner) has reserved other publication rights, and neither the thesis nor extensive extracts from it may be printed or otherwise reproduced without his/her written permission.

L'autorisation a été accordée à la Bibliothèque nationale du Canada de microfilmer cette thèse et de prêter ou de vendre des exemplaires du film.

L'auteur (titulaire du droit d'auteur) se réserve les autres droits de publication; ni la thèse ni de longs extraits de celle-ci ne doivent être imprimés ou autrement reproduits sans son autorisation écrite.

ISBN 0-315-45699-X

THE UNIVERSITY OF ALBERTA

RELEASE FORM

NAME OF AUTHOR:	Dalu PENG
TITLE OF THESIS:	THE MEASUREMENT OF ELECTROGASTROGRAM
DEGREE:	MASTER OF SCIENCE
YEAR THIS DEGREE GRANTED:	1988

Permission is hereby granted to THE UNIVERSITY OF ALBERTA LIBRARY to reproduce single copies of this thesis and to lend or sell such copies for private, scholarly or scientific research purposes only.

The author reserves other publication rights, and neither the thesis nor extensive extracts from it may be printed or otherwise reproduced without the author's written permission.

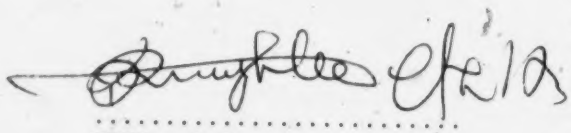

PENG, Dalu

Permanent Address:

Shanxi University

P.R. of CHINA

Date: July 6, 88

THE UNIVERSITY OF ALBERTA

FACULTY OF GRADUATE STUDIES AND RESEARCH

The undersigned certify that they have read, and recommend to the Faculty of Graduate Studies and Research for acceptance a thesis titled " Measurement of Electrogastrogram submitted by Dalu Peng in partial fulfilment of the requirements for the degree of M. Sc. in Department of Electrical Engineering.

Supervisor .....

.....

.....

.....

Date: 28 June 1988

ABSTRACT

The measurements of gastric electrical activities have been an important research area in the study of gastrointestinal motility. The gastroelectrogram (EGG) can be recorded by mucosal, serosal and cutaneous electrodes. In this research, a mathematical model to simulate EGG on the stomach with computer simulations is introduced. It is shown that the temporal and spatial characteristics of the EGG can be modeled of the gastric muscle level. Current mucosal EGG recording methods have been examined and several new types of mucosal EGG measurement techniques have been developed. The recordings using a balloon electrode assembly on canine stomach in in-vivo mucosal EGG measurements under anesthetization have shown that the temporal and spatial organizations of EGG can correctly be obtained. Human mucosal EGG measurements using the balloon electrode assembly have not yet been very successful; the reasons are given. A technique of using stainless steel clips to record mucosal EGG has been developed and tested on canine stomach, and human experiments have been designed.

We assume that there are magnetic fields associated with gastric electrical activities in stomach and the magnetogastrogram (MGG) can be measured on the surface of stomach wall. To support our assumption, a model of gastric magnetic fields based on a volume conductor model is introduced to show that generally two magnetic field orientations exist on the stomach muscle wall. Attempts of measuring MGG have been made using a Gaussmeter and preliminary results are given.

To measure simultaneous gastric contractile activities while measuring gastric electrical activities, a pressure gauge was used to record the pressure change in the balloon. From human and animal gastric contractile measurements, it has been shown that both weak and strong gastric contractions in antrum can be registered.

ACKNOWLEDGEMENTS

I wish to express my profound gratitude to Professor Y.J.Kingma and Professor K.L.Bowes for their invaluable direction, and to Dave.R, Paul.S. and Ken.C. for their great help.

CONTENTS

page

CHAPTER 1 INTRODUCTION.....1

1.1 THE HISTORY OF STUDIES OF GASTRIC ELECTRICAL AND MECHANICAL ACTIVITIES.....1

1.2 GASTRIC ELECTRICAL CONTROL ACTIVITY AND ELECTRICAL RESPONSE ACTIVITY.....6

1.3 RELATIONS OF ECA AND ERA IN STOMACH.....9

1.4 CLINICAL SIGNIFICANCE OF ECA AND ERA MEASUREMENTS.....12

CHAPTER 2 A MATHEMATIC MODEL OF ELECTROGASTROGRAM.....15

2.1 FORWARD PROBLEM OF GASTRIC ELECTRICAL CONTROL AND RESPONSE ACTIVITIES.....15

2.2 SUMMARY OF CHAPTER 2.....34

CHAPTER 3 MUCOSAL EGG ELECTRODE ASSEMBLY DESIGN AND SIGNAL MEASUREMENTS.....36

3.1 SUCTION MUCOSAL EGG ELECTRODE ASSEMBLY I.....36

3.2 SUCTION MUCOSAL EGG ELECTRODE ASSEMBLY II.....41

3.3 RING ELECTRODE ASSEMBLY.....45

3.4 BALLOON ELECTRODE ASSEMBLY I.....50

3.5 BALLOON ELECTRODE ASSEMBLY II.....59

3.6 CLIP MUCOSAL EGG ELECTRODE DESIGN AND EGG MEASUREMENTS.....64

3.7 SUMMARY OF CHAPTER 3.....68

CHAPTER 4 A STUDY OF MEASUREMENT OF MAGNETIC FIELDS IN INTACT ANTRUM.....69

4.1 INTRODUCTION.....69

4.2 A STUDY OF EXTRACELLULAR POTENTIAL AND MAGNETIC FIELDS OF ANTRUM SMOOTH MUSCLE: A FORWARD PROBLEM.....72

4.1.1 THE POTENTIALS.....72

4.1.2 MAGNETIC FIELDS.....81

4.3 A TENTATIVE DIRECT MEASUREMENT OF MAGNETOGASTROGRAM (MGG) IN CANINE STOMACH.....86

4.4 MUCOSAL MGG MEASUREMENTS.....90

4.5 SEROSAL MGG MEASUREMENTS.....94

4.6 DISCUSSIONS.....96

4.7 SUMMARY OF CHAPTER 4.....99

CHAPTER 5 MEASUREMENT OF GASTRIC CONTRACTILE ACTIVITY.....101

5.1 INRODUCTIION.....101

5.2 THE MEASUREMENT OF GASTRIC CONTRACTILE ACTIVITIES USING BALLOON ELECTRODE ASSEMBLY.....103

5.3 SUMMARY OF CHAPTER 5.....110

CHAPTER 6 OVERALL SUMMARY AND CONCLUSIONS.....112

LIST OF TABLES

PAGE

Table 1. Electrical control activity (ECA) and electrical response activity (ERA). 11

LIST OF FIGURES

		PAGE
Figure 1.1	Schematic diagram of stomach	3
Figure 1.2	Recording of gastric electrical control activity (ECA) in human stomach	7
Figure 1.3	Phases of canine gastric interdigestive myoelectric activity	10
Figure 2.1	Model of Human Torso	17
Figure 2.2	Vector Diagram	18
Figure 2.3.	Simulated electrogastrograms: Forward propagation	21
Figure 2.4.	Simulated electrogastrograms: retrograde propagation	22
Figure 2.5.	A schematic representation of antum by a truncated cone	24
Figure 2.6.	Simulated ECA at the surface of cone. Three pairs of points: (a) 8-7.8 cm; (b) 6-5.8 cm; (c) 4-3.8 cm from the vertex of the cone.	30
Figure 2.7.	Simulated cutaneous EGG on abdominal skin (a) on z' plane of the model. (b) in in-vivo recording.	31

Figure 2.8 ECA and ERA obtained from two points, 4 and 3.8 cm from the pylorus and the vertex of the cone respectively. 32

Figure 2.9 ECA and second component as obtained on the cone surface, at the point 8 cm from the vertex (monopolar recording). 33

Figure 3.1 A schematic diagram of mucosal suction electrode assembly I. 38

Figure 3.2. Ag/AgCl electrode impedance at different frequences (electrode area: 0.856 mm^2). 39

Figure 3.3. A canine mucosal EGG recording using suction electrode assembly I. 40

Figure 3.4 A schematic diagram of bipolar mucosal EGG suction electrode assembly II. 42

Figure 3.5. A canine mucosal EGG recording using suction electrode assembly II. 44

Figure 3.6 A schematic diagram of multichannel ring shape mucosal EGG electrode assembly. 47

Figure 3.7 A canine mucosal EGG recording using ring electrode assembly. 48

Figure 3.8. Balloon shape gastric electrode assembly I. 51

Figure 3.9. A schematic diagram of surface adhesion

measurement. 53

Figure 3.10 Surface adhesion vs electrode displacement. 54

Figure 3.11 A typical mucosal EGG measurement system. 56

Figure 3.12 A canine mucosal EGG recording using balloon electrode assembly I. 57

Figure 3.13 A human mucosal and cutaneous EGG recording using balloon electrode assembly I. 58

Figure 3.14 A schematic diagram of balloon electrode assembly II. 61

Figure 3.15 A human mucosal EGG using balloon electrode assembly II. 63

Figure 3.16 The clipsetter used in positioning clip electrode on antrum mucosal muscle through endscopic technique. 66

Figure 3.17 A canine mucosal EGG using clip electrode 67

Figure 4.1 Antrum is simulated as a long cylindrical object immersed in the internal and external media with conductivities σ_i and σ_e respectively. 73

Figure 4.2. A schematic diagram showing the moving dipole band, current density and associated magnetic fields. 87

Figure 4.3. A mucosal MGG measurement system 91

Figure 4.4. A mucosal MGG recording in intact canine stomach. 93

Figure 4.5. A serosal MGG recording in intact canine stomach. 95

Figure 4.5a FFT of serosal EGG 97

Figure 4.5b FFT of serosal MGG 98

Figure 5.1. A schematic diagram of gastric introluminal pressure measurement system. 104

Figure 5.2. Simultaneous measurement of gastric mucosal EGG and gastric introluninal pressure in canine stomach. 106

Figure 5.3. A recording of human EGG, gastric intraluminal pressure and respiration. It is shown that the trace E has the same frequency as that of EGG's. 108

Figure 5.4. A recording of human mucosal EGG, gastric intraluminal pressure and respiration. It is shown that the gastric contraction occurs at a lower frequency than that of EGG's. 109

CHAPTER 1

1 INTRODUCTION

1.1 THE HISTORY OF GASTRIC ELECTRICAL AND MECHANICAL ACTIVITIES

Since the studies of Alvarez[2] on mammalian gastric electrical activity, the nature of gastric rhythmicity has held the interest of many gastrointestinal investigators[1]. It is unknown who first observed the contractions of the human stomach, but early studies of gastrointestinal activity were made in the late 1800's and early 1900's, The first well known study of human stomach electrical activity made by Alvarez[2,3] using a calomel type electrode in contact with the serosal surface of the stomach indicated that a gastric ccntraction is usually a mechanical manifestation of an electrical event. Since then the regions of the stomach were

further detailed in terms of their electrical activities and mechanical activities[4-11,17-19]. The stomach can be divided, in general, into three regions:

1) fundus

This is the most orad portion of the stomach, which does not show regular pacemaker potentials.

2) corpus

This is the central portion of the stomach; it exhibits regular pacemaker potentials[3-9]. The corpus can also be subdivided into orad, mid, and caudad corpus.

3) antrum

This is the most distal part of the stomach with a length of approximately 7 to 8 cm. It presents strong rhythmic potentials, and these potentials are often superimposed with spike potentials[8-10]. The antrum can be divided into orad and terminal antrum. A schematic diagram of the regions of human stomach is given in Figure 1.1.

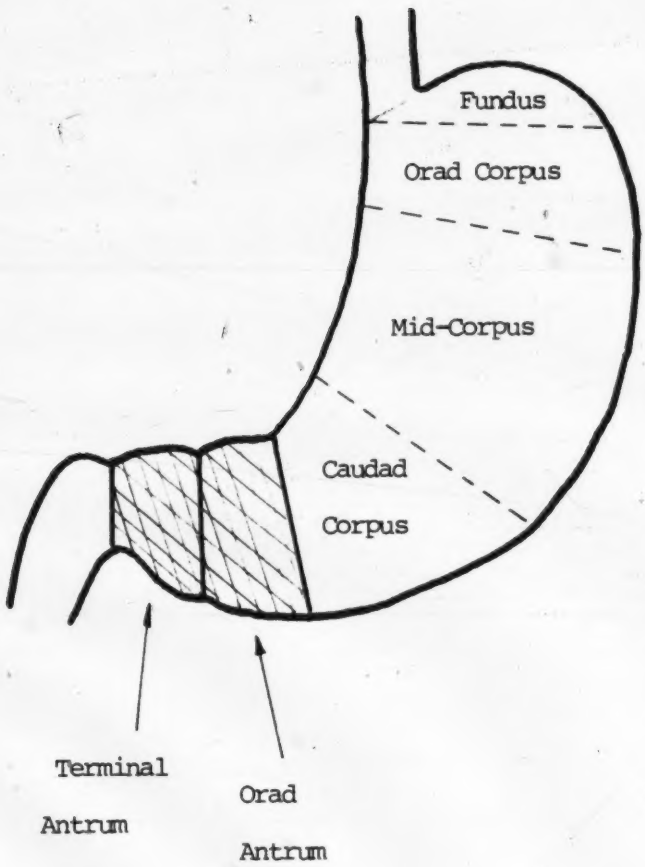

Figure 1.1 A Schematic Diagram of Human Stomach

Following the work of Alvarez in the 1920's, extensive research has been done both on animal and human stomach. The electrical and mechanical activities were further defined [4-7,10,11,15-16]. These studies revealed that there is a region in the mid corpus of the stomach that functions as the gastric pacemaker [4,5,11-12]. The spontaneous cyclical changes in potential in the pacemaker region determine the frequency of the gastric electrical control activity (ECA). The electrical response activity (ERA) corresponds to the contractile activity in stomach. When it exists it is coincident with ECA, but it is not omnipresent. Rather, it is in phase with ECA and its frequency can not exceed that of ECA's. The controls of ECA are neural, hormonal, and perhaps paracrine[4]. The general properties of gastric ECA and ERA will be further examined in the next sections.

The electrogastrogram (EGG) can be recorded intracellularly, extracellularly and extracutaneously. The extracellular EGG recordings have been obtained with both surgical and nonsurgical techniques, such as sutured serosal electrodes and mucosal electrodes respectively. The waveforms of extracellular EGG recordings are not identical with those of intracellular ones. The differences may be explained in part by cable theory [5], which states that the extracellular EGG

signals approximate the first time derivative of the intracellular action potentials [6]. In in-vivo recordings, if the effects of artifacts are excluded, the EGG waveforms are more likely affected by the following:

1) electrode configurations

Indeed, the electrode configurations do affect the serosal EGG waveforms. The bipolar electrode configuration of serosal EGG recordings represents the difference of adjacent measuring points in the stomach muscle. The waveforms are typically similar to the second time derivative of the stomach muscle action potentials. While the monopolar serosal EGG referenced to a remote neutral electrode, in contrast, yields the first time derivative of the action potentials.

2) EGG recording methods

With the same electrode configuration, for example a bipolar electrode configuration, the waveforms of recorded EGG vary with recording methods. That is, the recording with the mucosal bipolar electrode configuration will show different EGG waveforms different from those of the serosa and the skin. It is possible that an integrating process may be involved in

the conduction of action potentials throngh the surrounding media.[9]

3) electrode-muscle contact

The EGG waveforms of mucosal recordings are affected by the electrode-muscle contact[12,14]. It is likely that good and stable electrode-muscle contact will result in greater signal altitude and higher signal to noise ratio.

1.2 GASTRIC ELECTRICAL CONTROL ACTIVITY AND ELECTRICAL RESPONSE ACTIVITY

In normal human stomach, the pacemaker potentials originate along the greater curvature of the stomach near the junction of orad and mid third of the corpus[4,5,11]. This cyclic activity of pacemaker potentials is found throughout the distal stomach. A bipolar recording of pacemaker potential is shown in Figure 1.2. The major effect of this pacemaker potential is to coordinate the activities of the distal gastric smooth muscle cells, so that a temporally

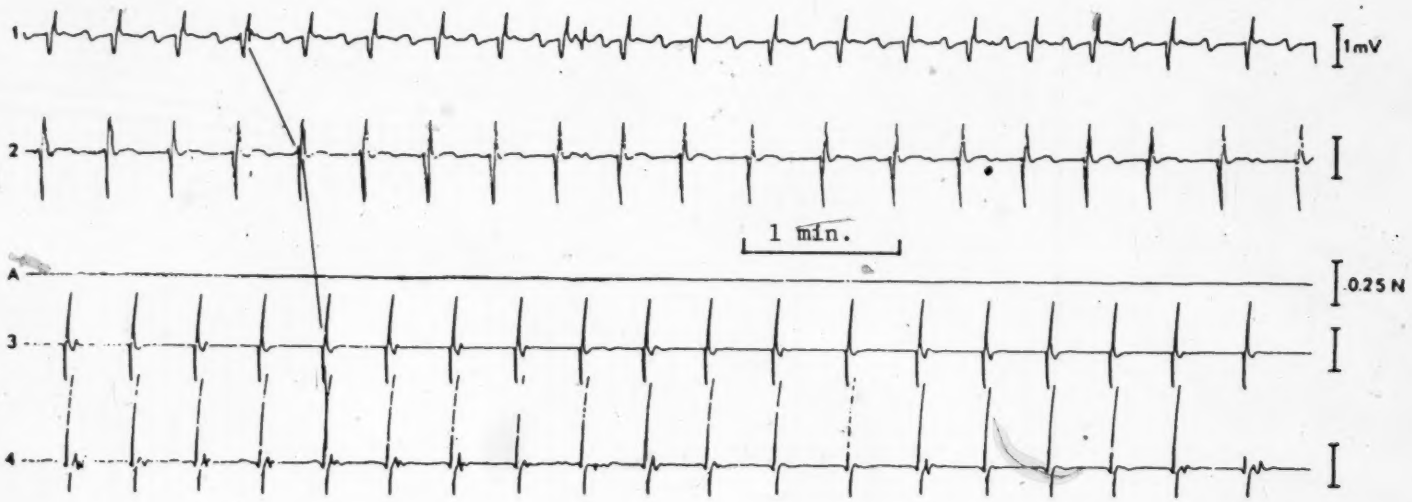

Figure I.2 Recording of gastric electrical control activity (ECA)
in human stomach

and spatially regular series of peristaltic waves sweeps aborally through the distal stomach to the terminal antrum[5]. This is the phenomenon that is sometimes called the electrical control activity (ECA). More precise experiments[9] suggest that each time the pacemaker potentials sweep through the distal stomach, they bring the gastric smooth muscle cells to the threshold of generating contractions. The threshold is exceeded briefly at the peak of the initial depolarization of pacemaker potentials [4,5,9,]. Since the pacemaker potential entrains the entire distal stomach, in any part of the distal stomach, the ECA has an identical frequency. This conclusion is supported by the fact that the distal stomach has greater excitability, or in other words the antral stomach has lower threshold and shorter refractory period than those of the corpus. Therefore, this property allows the antrum to be more readily driven[9-11]. The ECA can be simulated either by an array of bidirectionally coupled relaxation oscillators[11] or by a moment of dipole band propagating on the surface of a truncated cone[17-19]. The intrinsic frequency of individual oscillators declines from greater to lesser curve as well as from orad corpus to terminal antrum in the relaxation oscillator model, and the dipole density increases from corpus to terminal antrum in a truncated cone model[17]. As a counterpart of ECA,

the electrical response activity (ERA) plays a key role in the gastrointestinal motility. The ERA does not occur by itself, however, it is controlled by ECA and other factors[4,6,10]. The ERA is believed to be responsible for large contractions of the stomach muscle [5,11]. ERA always occurs in phase with ECA and its frequency of occurence can not exceed that of ECA's. Like that of ECA in stomach, ERA is also a temporal and spatial event.

1.3 RELATIONS OF ECA AND ERA IN STOMACH

There is a period of interdigestive myoelectrical complex (IMC) in the stomach during fasting[9], in which sequentially arranged features of myoelectrical activity occur throughout the terminal stomach[4]. As an example, a recording of three major phases of interdigestive myoelectrical activity is shown in Figure 1.3[9]. During phase 1, no spike potentials and corresponding contractions occur in the gastric wall[9]. Only ECA manifests itself during phase 1 and it usually lasts 45 to 60 minutes; phase 2 is marked by intermittent spike potentials and corresponding contractions.

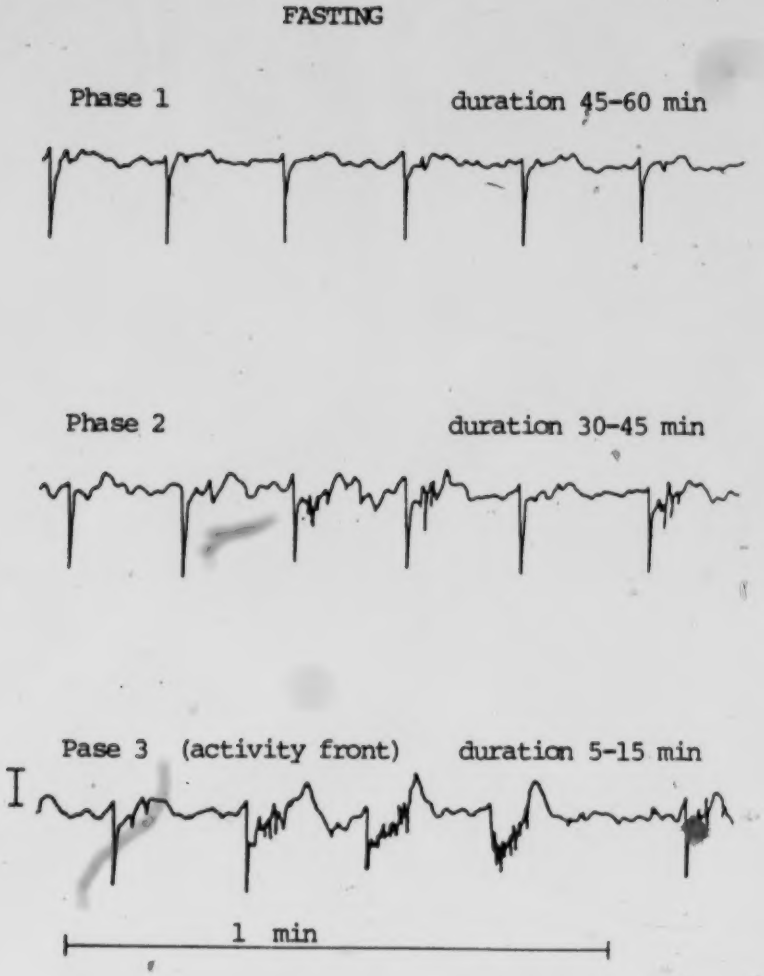

Figure 1.3 Phases of canine gastric interdigestive myoelectric activity

TABLE 1. ELECTRICAL CONTROL ACTIVITY (ECA) AND ELECTRICAL RESPONSE ACTIVITY (ERA)

ECA	ERA
* A temporal and spatial electrical event	* A temporal and spatial electrical event
* Cyclic depolarization usually without muscle contractions	* Contractions with spike action potentials
* Frequency is set by gastric pacemaker potentials	* Frequency can be as high as that of ECA's
* Propagating distally	* Propagating distally
* Controlled by neural, hormonal or perhaps paracrine	* Controlled by ECA
* Always presents in stomach	* Occuring during the feeding and IMC during fasting

That is, the ERA becomes active in this phase. Phase 2 usually lasts about 30 to 45 minutes; By the end of phase 2, the incidence of ERA gradually increases which marks the onset of phase 3. Intense spike potentials occur with each pacemaker potential in antrum in phase 3. During phase 3, strong peristaltic contractions prevail. Strong proximal gastric tonal contractions occur as well[4,5,8]. Phase 4 is a 5-minute transition phase between phase 3 and the next complex cycle. ECA and ERA are coordinated in such a way during the interdigestive myoelectrical complex that the emptying of the indigestible debris begins in phase 2 and is completed by phase3 [9]. The fasting IMC cycles are immediately abolished with the feeding. Both nerves and hormones play a role in this abolition [4,5,8,9]. During feeding, ECA and ERA are coincident in time and space. As a consequence, the regular peristaltic contractions dominate the antrum during feeding.

1.4 CLINICAL SIGNIFICANCE OF ECA AND ERA MEASUREMENTS

In normal human stomach the ECA frequency is approximately 3 cycles per minute. The ERA ranges from 0 to 3 cycles per minute. The rhythm of ECA is remarkable stable, with little day to day variation[4]. A number of gastric disorders related to the abnormal gastric ECA and ERA signals were reported [15,16]. Two types of abnormal ECA are:

1) tachygastria characterized by an increased frequency of ECA and

2) tachyarrhythmia in which the ECA is faster but has irregular periods and configurations [16].

Current research has added more evidence showing that a number of human stomach abnormalities, such as unexplained nausea, epigastric bloating and vomiting[16] can be studied using ECA and ERA measurements.

In one of our experiments, a constipated patient showed an irregular ECA, reversal of ECA propagation and some possible regional ECA uncoupling. However, why and how the ECA and ERA are disturbed by gastric pathological changes is not

fully understood. Some chemicals, such as adrenaline, atropine, morphine and large doses of histamine induce antral arrhythmias[13]. The antral arrhythmia may correspond to the dominance of sympathetic over parasympathetic activities [4,5,8]. ECA and ERA have shown great clinical significance in gastrointestinal motility research. However more extensive work has to be done before wider acceptance of its diagnostic value is gained.

CHAPTER 2

2.1 FORWARD PROBLEM OF GASTRIC ELECTRICAL CONTROL AND RESPONSE ACTIVITY

A very important aspect in the EGG studies is the simulation of gastric electrical activities.

A number of mathematical models have been suggested in the literature. Plonsey[20-23] has proposed a volume conductor model to describe the characteristics of a myogenic current source in a conductive medium and later this model was developed to represent a current source in the antrum of a human torso which can be represented as[32]:

$$\nabla^2 \phi(\underline{r}, t) + K^2 \phi(\underline{r}, t) = - \frac{I\delta(\underline{r} - \underline{v}_o t)}{\sigma + j\omega\epsilon} \qquad -2.1-$$

[see Figure 2.1]

and if we assume a stationary current source to approximate the moving myogenic current source as shown in Figure 2.1, equation 2.1 is reduced to:

$$\nabla \phi^2 + K^2\phi = \frac{-I}{\sigma + j\omega\epsilon} \qquad -2.2-$$

which can be solved as a solution in an infinite medium:

$$\phi_\infty = \frac{1}{4\pi\sigma_o} \int_v \frac{I}{\underline{R}} e^{-jk\underline{R}} dv \qquad -2.3-$$

where $\underline{R} = \underline{r} - \underline{r}_o$ as shown in Figure 2.2 and $e^{-jk\underline{R}}$ are the propagation delay. Equation 2.3 is only an approximation of the system. Firstly, because of both conductive and dielectric properties, it will take a finite time for the source signal at a given point to register at far field. Secondly, since the system is nonisotropic a single change in a field may arrive at the same observation point with different time delays due to multiple signal paths. However Plonsey has shown

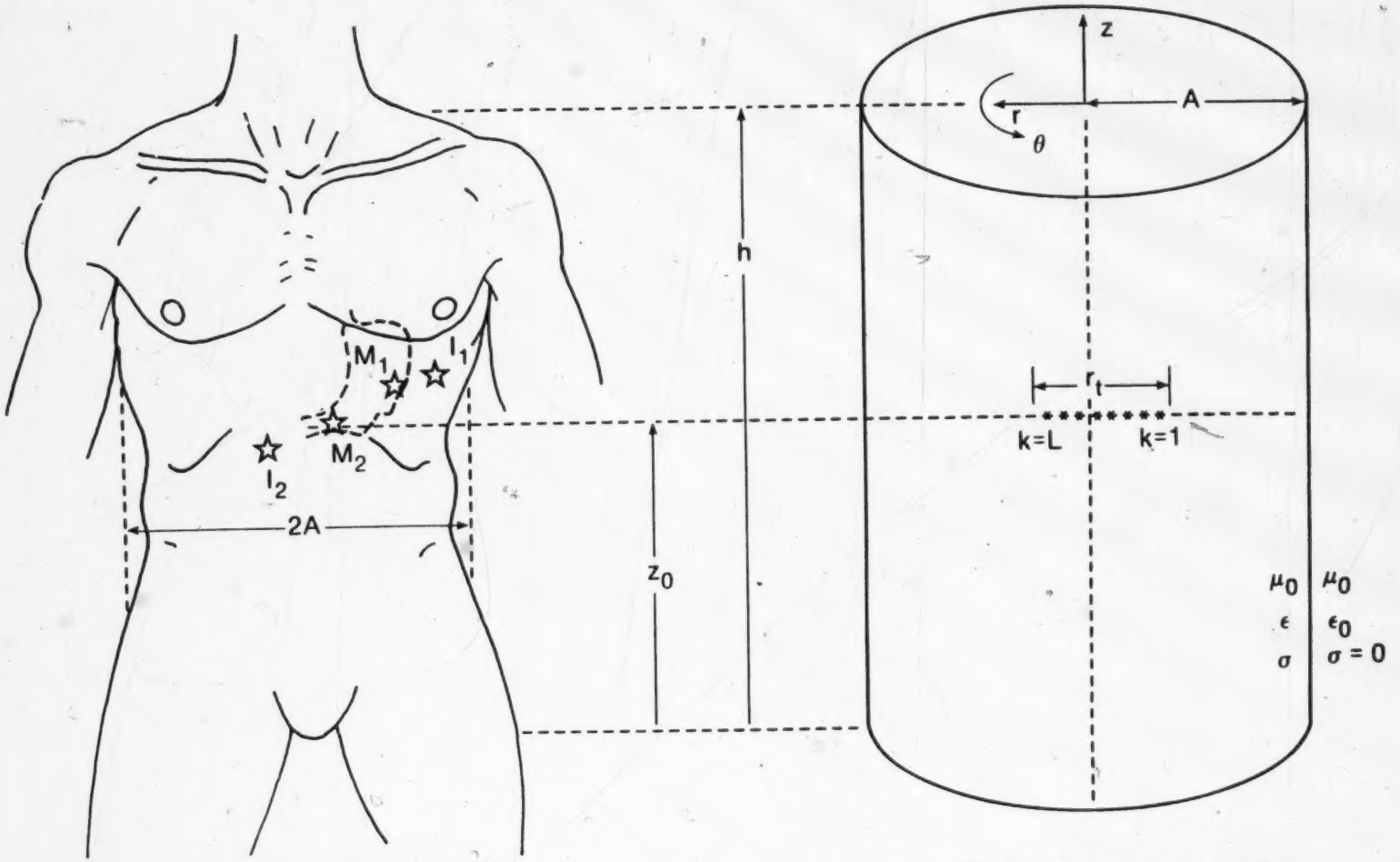

FIGURE 2.1

Model of Human Torso

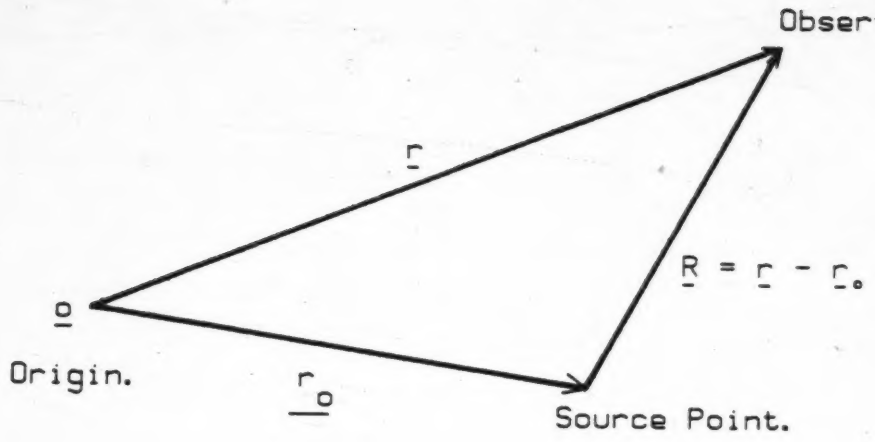

FIGURE 2.2

VECTOR DIAGRAM.

that equation 2.1, 2.2 and 2.3 in fact are good approximations of the real system by neglecting capacitive, inductive and propagation effects [21].

In recent work, Familoni [32] has shown a model that describes both temporal and spatial properties of the volume conductor system. By replacing the current source by a single moving dipole(SMD) of moment P:

$$P = (P_r, P_\theta, P_z,) \qquad -2.4-$$

to show the surface potential of the torso we have:

$$\phi = \phi_r + \phi_\theta + \phi_z \qquad -2.5-$$

assuming that the system is quasistatic, Laplace's equation can be solved. Finally, the finite volume conductor solution can be obtained by the method of images [23]. By imposing the boundary functions [22], equation 2.4 and 2.5 can be solved in the form of Bessel's functions in infinite order.

Since the solutions of equation 2.5 are not presented in closed form, it is likely that quantitive interpretation will suffer as well, The direct computer simulation of the model may be difficult due to the Bessel functions in this solution being of infinite order. Figure 2.3 and 2.4 present simulated cutaneous EGG's using this model[32].

It is known that the EGG can be measured not only on the stomach muscle wall, but on the abdominal skin as well. We need a model that can simultaneously predict mucosal EGG, serosal EGG, and cutaneous EGG. This model should also be able to predict ERA and EGG morphological characteristics in the in-vivo experiment, such as waveforms, amplitude, frequency and phase lag. Mirizzi[17] has suggested a model that satisfies the requirements shown above. It is known that there are periodic potential changes produced from mid corpus to pylorus in human stomach [4-9]. Firstly, if we assume that the stomach between corpus and pylorus is symmetrical to its central axis, then this portion of the stomach can be well simulated by a truncated cone of finite length [19]. Secondly, the temporal and spatial properties of gastric electrical activities (ECA and ERA) can also be represented on the stomach muscle wall by an annular

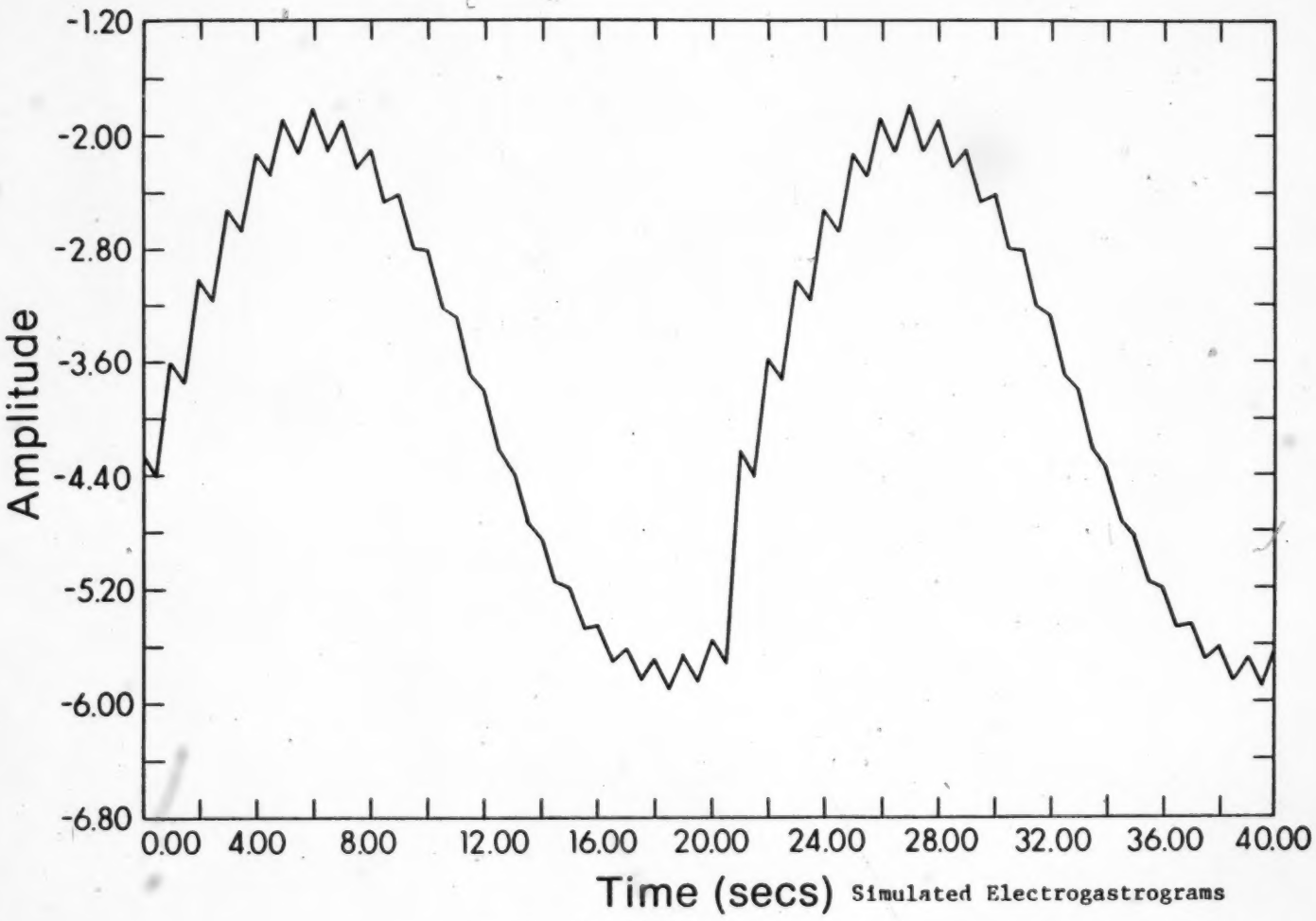

Simulated Electrogastrograms

FIGURE 2.3 Forward Propagation

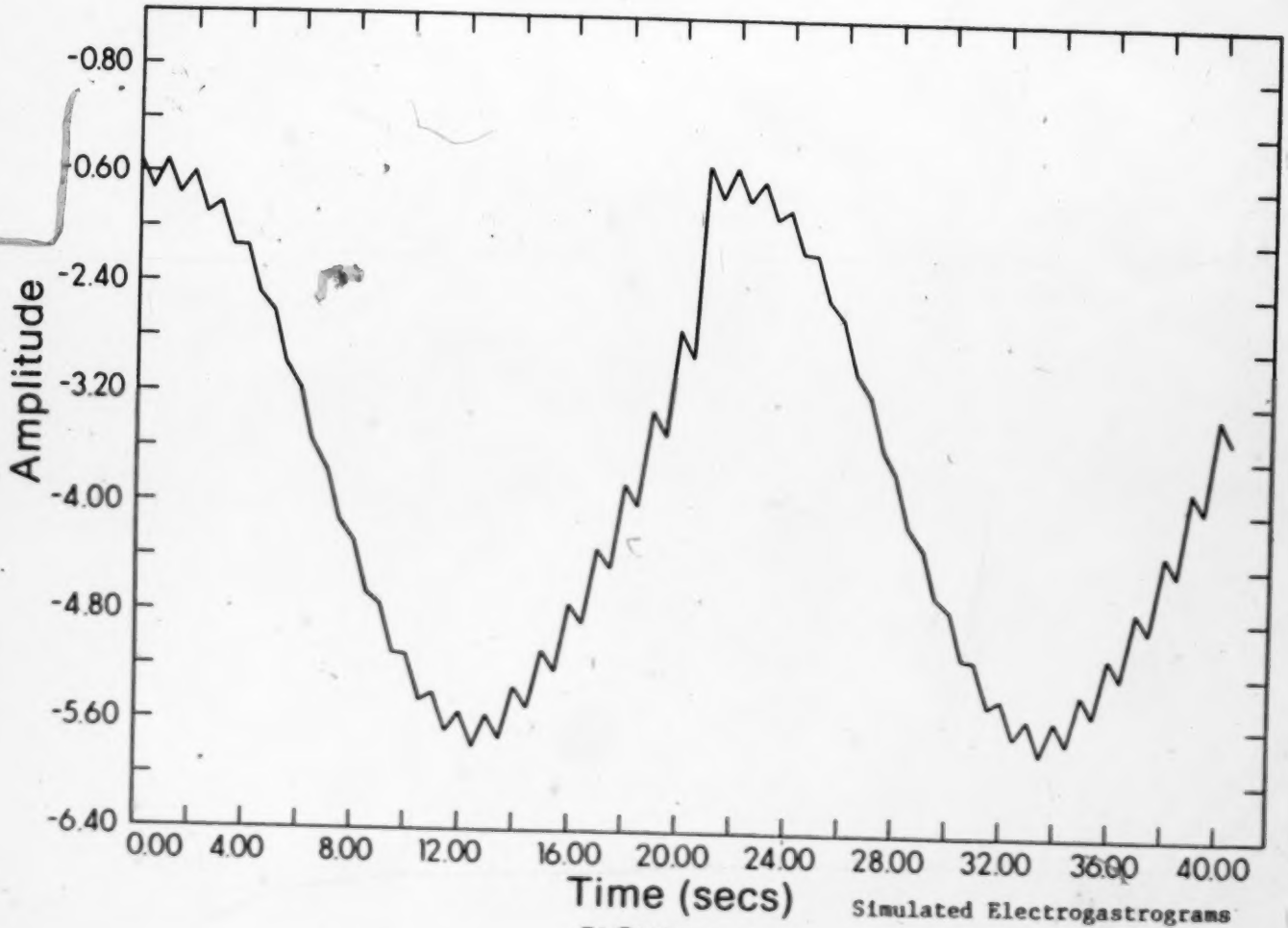

Simulated Electrogastrograms

FIGURE 2.4

Retrograde Propagation

depolarized dipole band, δ in width, moving distally to the cone vertex. A schematic diagram of distal stomach simulation by a truncated dipole cone is shown in Figure 2.5.

In Figure 2.5, Q is a generic point in space, ds represents a dipole cell of infinitesimal area on moving dipole band, $\underline{P}$ is the dipole moment vector perpendicular to the cone surface. Thus, the potential produced by the band of dipole moment observed at point Q can be expressed in a polar coordinate system as:

$$\underline{V}(\underline{r}) = \frac{1}{4\pi\epsilon_o} \iint_s \frac{\underline{D} \cdot (\underline{r} - \underline{R})}{|\underline{r} - \underline{R}|^3} \, ds \qquad -2.6-$$

where $\underline{D}$ is the dipole density of the annular polarized dipole band. For convenience of computer simulation, we need to convert the polar coordinates into rectangular coordinates. These transformations are performed as follows:

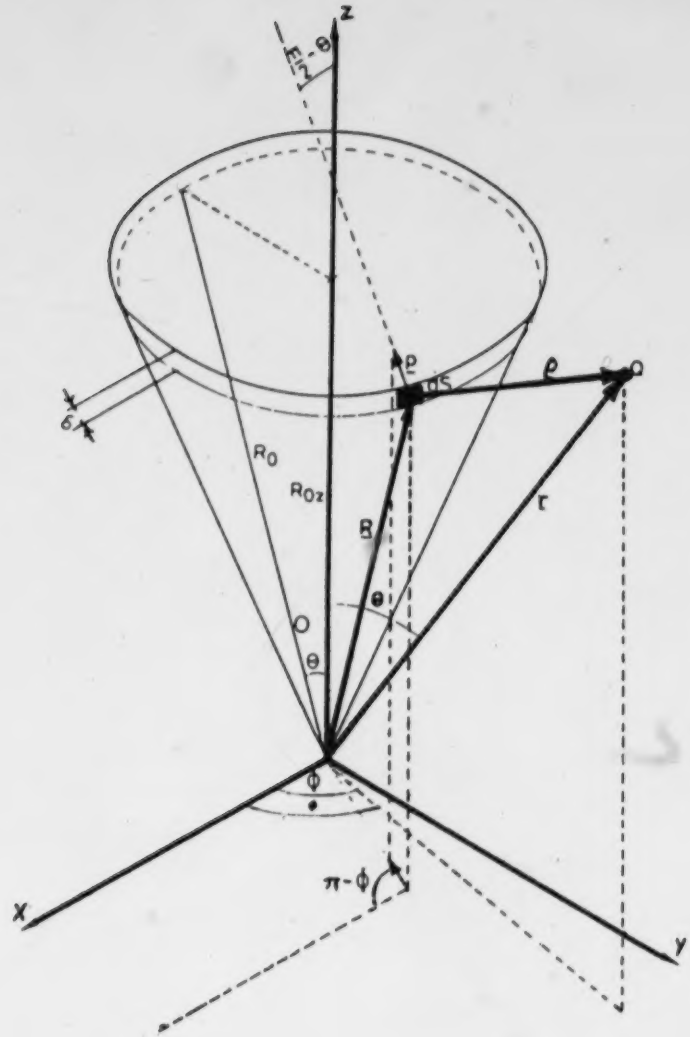

Figure 2.5 schematic representation of antrum by a truncated cone

$$X_R = R \sin\theta \cos\Phi$$
$$Y_R = R \sin\theta \sin\Phi \qquad \text{-2.7-}$$
$$Z_R = R \cos\Phi$$

and

$$X_r = r \sin\theta \cos\phi$$
$$Y_r = r \sin\theta \sin\phi \qquad \text{-2.8-}$$
$$Z_r = r \cos\theta$$

and

$$X_p = -\rho \cos\theta \cos\Phi$$
$$Y_p = -\rho \cos\theta \sin\Phi \qquad \text{-2.9-}$$
$$Z_p = \rho \sin\theta$$

Where the polar coordinates for vector $\underline{P}$ are ρ, $\pi/_2$ and $\pi - \Phi$.

As the moment P equals to the product of dipole density D and the infinitesimal area ds, the scalar product $\underline{P} \cdot (\underline{r} - \underline{R})$ can be written:

$$\underline{P}\cdot(\underline{r}-\underline{R}) = -Pr[\sin\theta\cos\Theta\cos(\Phi-\phi)-\sin\Theta\cos\theta] \qquad -2.10-$$

and

$$|\underline{r}-\underline{R}| = (r^2+R^2-2rR[\cos\theta\cos\Theta+\sin\theta\cos(\Phi-\phi)\sin\Theta])^{3/2} \qquad -2.11-$$

equation 2.6 then becomes:

$$V(r,\ \theta,\ \phi) = \frac{-D}{4\pi\epsilon_o} \int_o^{2\pi} \int_{RO}^{RO+\delta}$$

$$\cdot \frac{r[\sin\theta\cos\Theta\cos(\Phi-\phi)-\cos\theta\sin\Theta]\sin\Theta R d\Theta d\Phi}{\{R^2-2rR[\cos\theta\cos\Theta+\sin\theta\sin\Theta\cos(\Phi-\phi)]+r^2\}^{3/2}}$$

-2.12-

To simulate this model on a computer, certain rules apply to equation 2.12.

a) the dipole band should move aborally with the increase of propagation velocity. This restriction is expressed by:

$$Z(t) = a\ [\ \exp\ (t/b) - 1\ ] + ct \qquad \text{-2.13-}$$

where a, b and c are constants to be determined.

b) the dipole density should vary distally. This restriction is expressed as:

$$D(t) = Po \,/\, S\,[Z(t)] \qquad \text{-2.14-}$$

where Po is the initial dipole moment. It is a constant throughout the cone surface, and S[Z(t)] is the area of the annular dipole band at time t on the cone surface.

The area S[Z(t)] is governed by:

$$S[z(t)] = \pi \{[\, R(t) + \delta]^2 - R^2(t)\} \sin\theta \qquad \text{-2.15-}$$

with $$R(t) = [\, R_{oz} - Z(t)] / \cos\theta \qquad \text{-2.16-}$$

where R_{oz} is the initial position of the annular dipole band on the cone.

The following parameters were chosen for the computer simulation[17]:

$R_{oz} = 15$ cm $\quad \theta = 20^{o}$ $\quad \delta = 3 \times 10^{-3}$m

$P_o = 2.2 \times 10^{-6}$ cm $\quad a = 30 \times 10^{-6}$m

$b = 2.5$ s and $c = 0.3$ cms^{-1}

These simulated bipolar ECA's on the cone surface, 4; 6 and 8 cm from the vertex, are in good agreement with bipolar ECA's measured in in-vivo experiment.

A sample of the bipolar ECA on the cone wall is shown in Figure 2.6. We noticed, from Figure 2.6, that the simulated bipolar ECA's possess temporal and spatial characteristics simular to those of in-vivo experiments. By representing the abdominal skin by a plant z' in this model, a simulated cutaneous EGG is given in Figure 2.7. The ERA signal, as pointed out by Mirizzi[17] , can also be simulated by this model. By modifying the dipole P , the constant b and the time length, the spike potentials superimposed on the bipolar

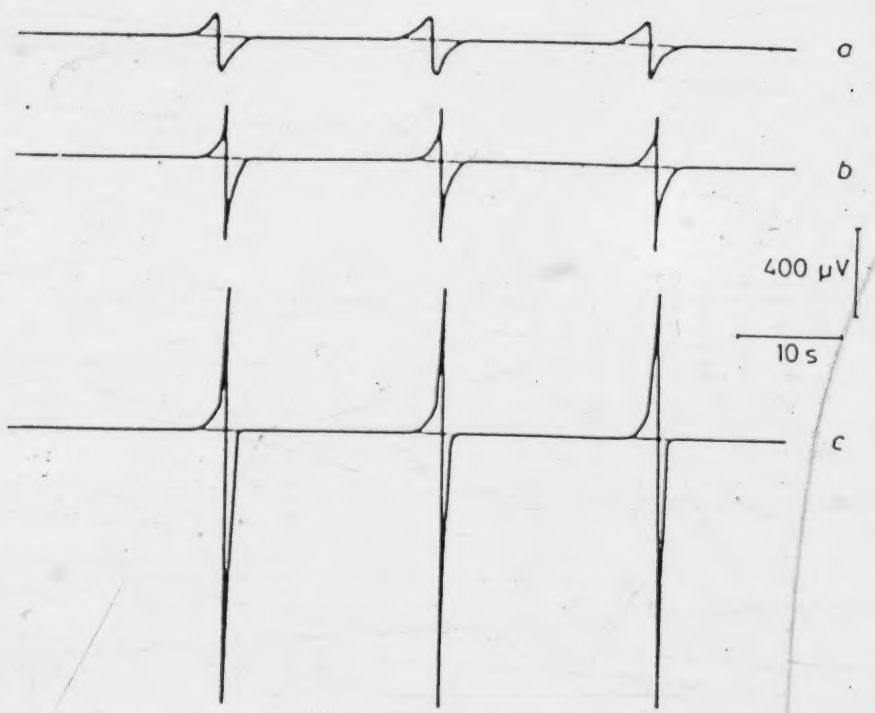

Fig 2.6 The simulated ECA at the surface of cone. Three pairs of points: (a) 8-7.8 cm (b) 6-5.8 cm (c) 4-3.8 cm from the vertex of the cone

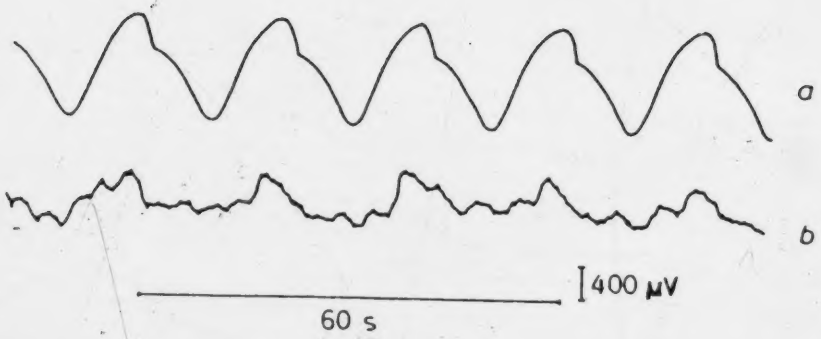

Fig 2.7 The simulated cutaneous EGG on abdominal skin
(a) on Z' plane of the model
(b) in in-vivo recording

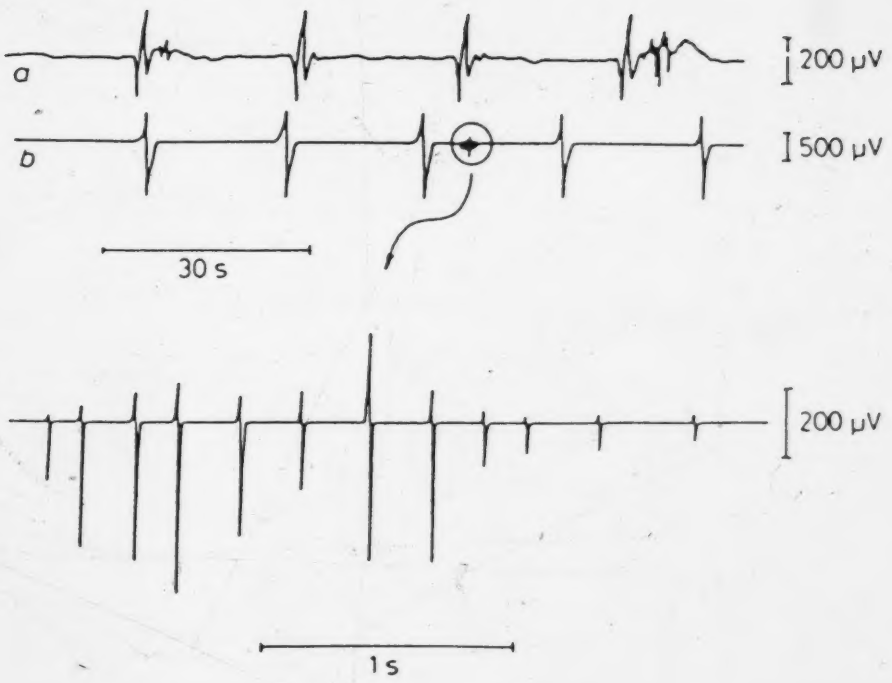

Figure 2.8 ECA and ERA obtained from two points, 4 and 3.8 cm from the pylours and the vertex of the cone respectively

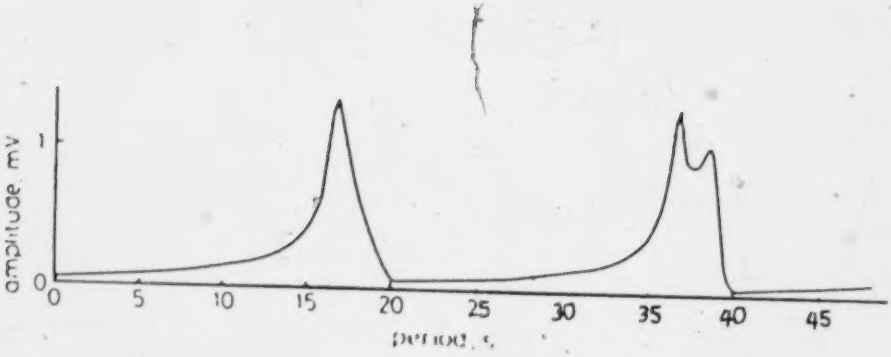

Fig 2.9 ECA and second component as obtained on the cone surface, at the point 8 cm from the vertex (monopolar recording)

ECA is reproduced as shown in Figure 2.8. As well, an output of monopolar ECA and the second component in the cone wall, 8 cm from the vertex is given in Figure 2.9. We emphasize that the model discussed here concerns only the muscle level simulation, that is, the ECA and ERA variation along the muscle thickness direction has not yet been taken in account. Therefore this model states that it makes no difference whether ECA is recorded on the cone wall at serosal side or mucosal side. This conclusion is obviously not true in in-vivo experiment.

2.2 SUMMARY OF CHAPTER 2

Previous models [20-23] fit well on cellular level of polarization and depolarization of muscle cell. Since then, a lot of effort has been made to extend this model to muscle strip and an organ. However, the mathematics involved in these models is so complex that direct computer simulation and interpretation are not all that straight forward. The model presented by Familoni[32] yields a fair prediction of cutaneous EGG, but the details of ECA and ERA characteristics in temporal and spatial domain are obscure and the direct computer simulation of the model is deterred by the mathematical complexity.

We found that the model introduced in this chapter possess advantages over other models:

(a) both ECA and ERA can be predicted by this model.

(b) the model is mathematically simple and can be simulated directly on the computer.

(c) both bipolar and monopolar signals can be predicted on both muscle wall and abdominal skin.

CHAPTER 3

3.1 MUCOSAL EGG ELECTRODE ASSEMBLY DESIGNS AND MEASUREMENTS

In this chapter, we will investigate a number of mucosal EGG electrode assembies developed and tested in this research. Since the mucosal EGG measurement is considered to be a minimally invasive technique, its improvement should immediately benefit clinical applications.

3.1 SUCTION MUCOSAL EGG ELECTRODE ASSEMBLY I

For this type of electrode assembly, the design considerations are based on work of Familoni [32], who developed a type of suction electrode assembly. The electrodes move outward when suction is applied. In our design several changes have been made:

(a) The radial size was reduced from 8 mm to 5 mm. The size of this assembly makes it possible to apply it as a pernasal electrode assembly.

(b) For the electrode body, instead of using a rigid plastic tube, a flexible rubber tube was used.

(c) electrodes were mounted in the center of each suction orifice, and glued on the bottom side.

(d) as shown in the Figure 3.1, the centre lines of both sides of the tube are made into two shallow grooves which guide the tube folding direction when suction is applied.

A, B, C and D are four Ag/AgCl electrodes[13], 1 mm in diameter, 4 mm in length, electrically isolated with shrinkable tubing. The tips of the electrodes are polished and then roughened. A layer of silver-silver chloride is then deposited. A diagram of typical electrode impedance vs frequency is given in Figure 3.2[13].

This type of electrode assembly has been applied on the stomach of anesthetized dogs. A sample of the canine gastric monopolar mucosal EGG is given in Figure 3.3. From the experiments, we found that this electrode assembly has a poor

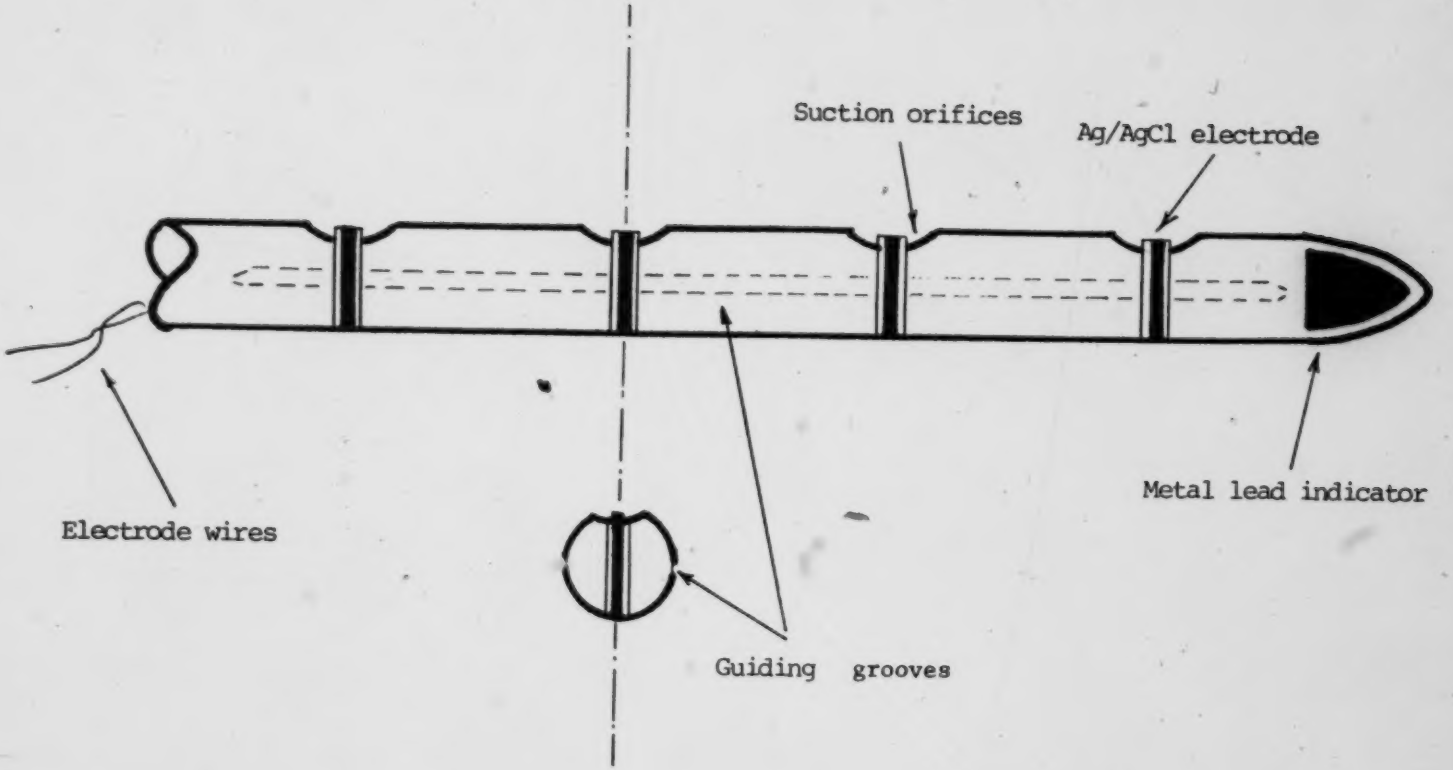

Figure 3.1 A schematic diagram of mucosal suction electrode assembly I

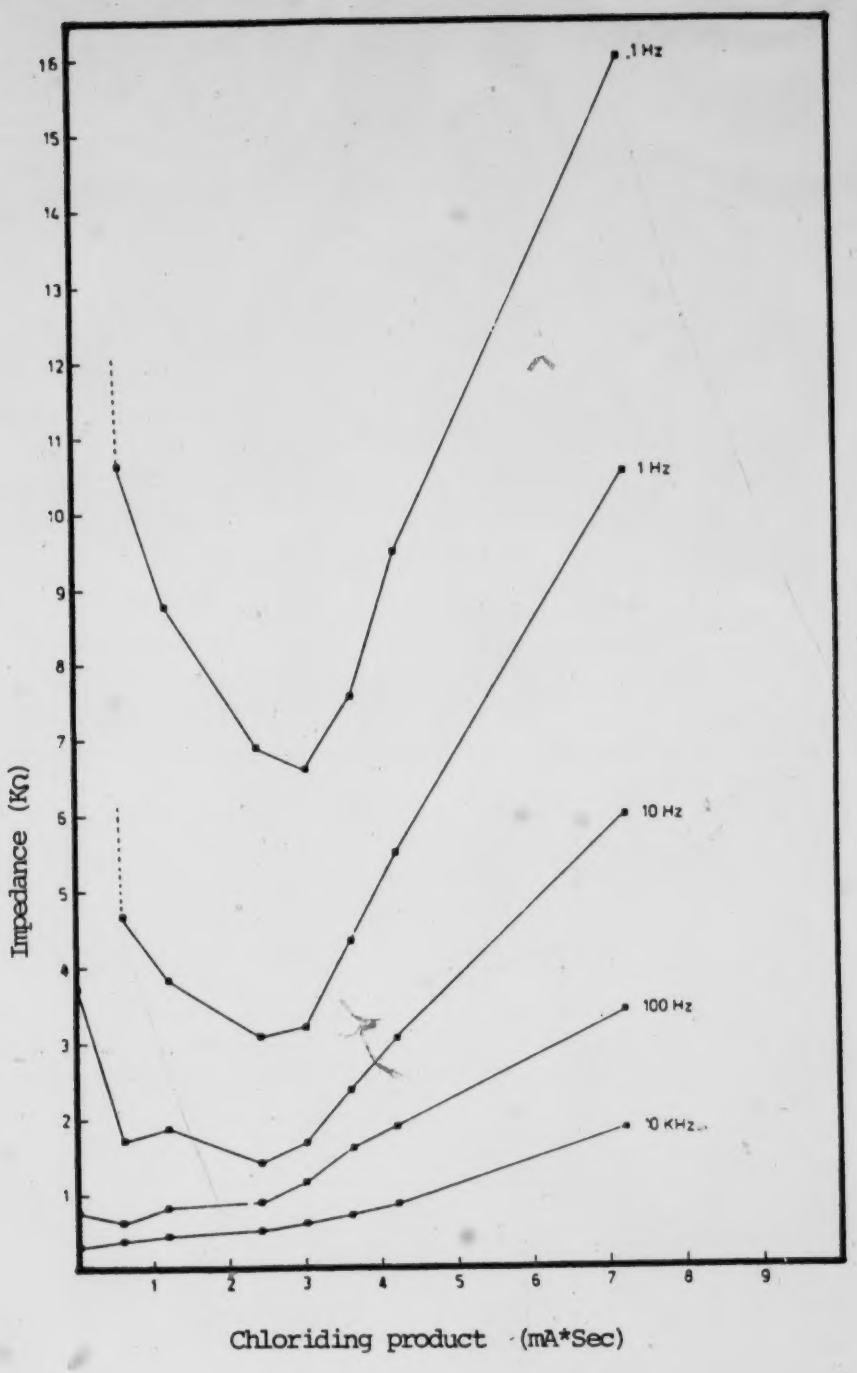

Figure 3.2 Ag/AgCl electrode impedence at different frequencies (electrode area: 0.856 mm^2)

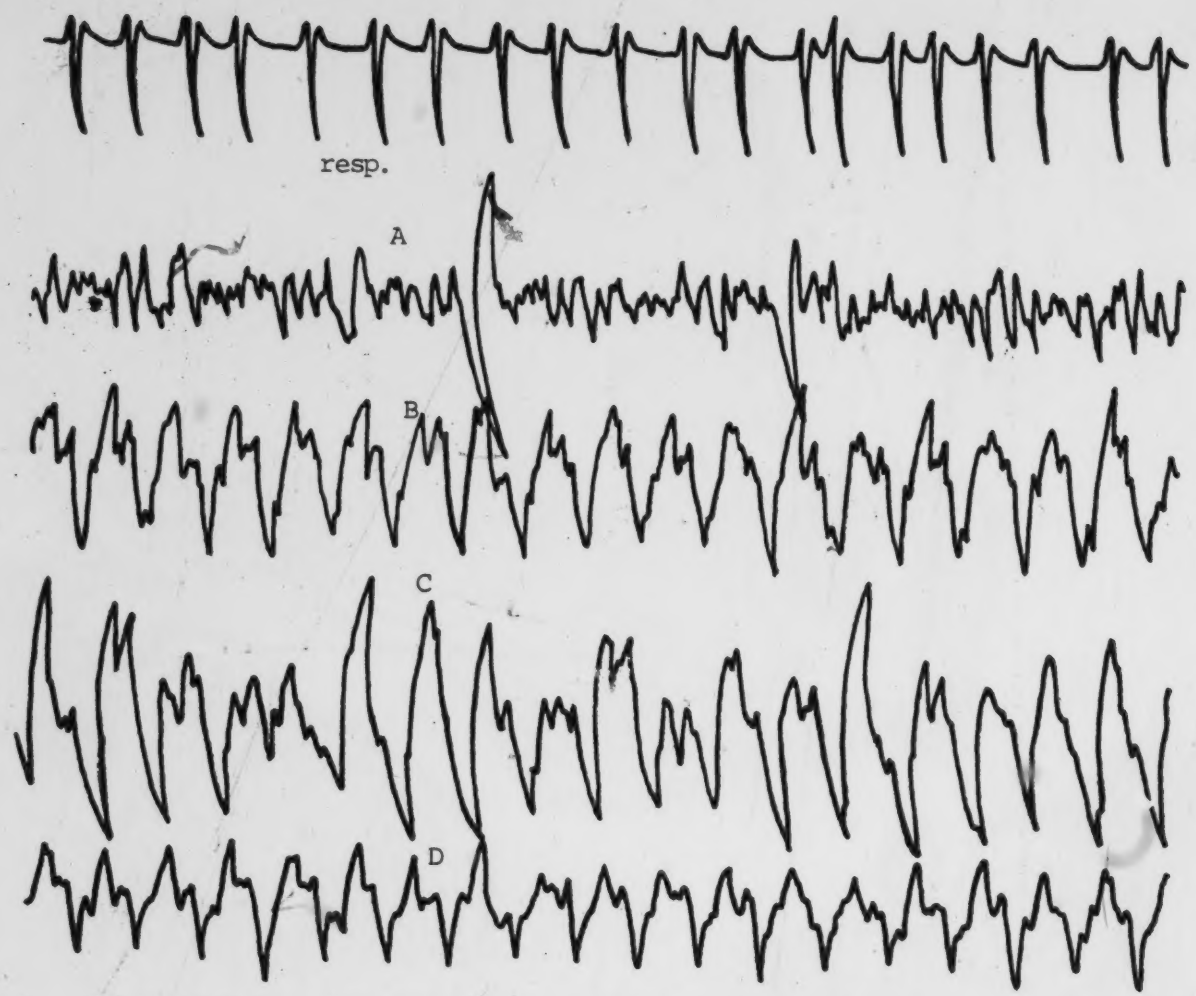

Figure 3.3 A canine mucosal EGG recording using suction electrode assembly

signal to noise ratio. Stable signal traces are seldom maintained for more than 20 minutes. The artifacts may be explained as follows:

(a) The mucosal muscle on one or more suction orifices may deteriorate and suction can not be effectively applied . As a result, the electrode assembly may fall off during the measurement.

(b) The mucosal muscle may be pulled away from circular muscle by suction. This reduces the signal amplitude and tends to be more noisy.

(c) Strong gastric contraction may cause electrode-mucosa separation or tear the mucosal muscle.

3.2 SUCTION ELECTRODE ASSEMBLY II

To improve the performance of suction electrode assembly I, we designed bipolar suction electrode assembly II. Figure 4.4 shows a schematic diagram of this assembly. The following changes were made for this electrode assembly:

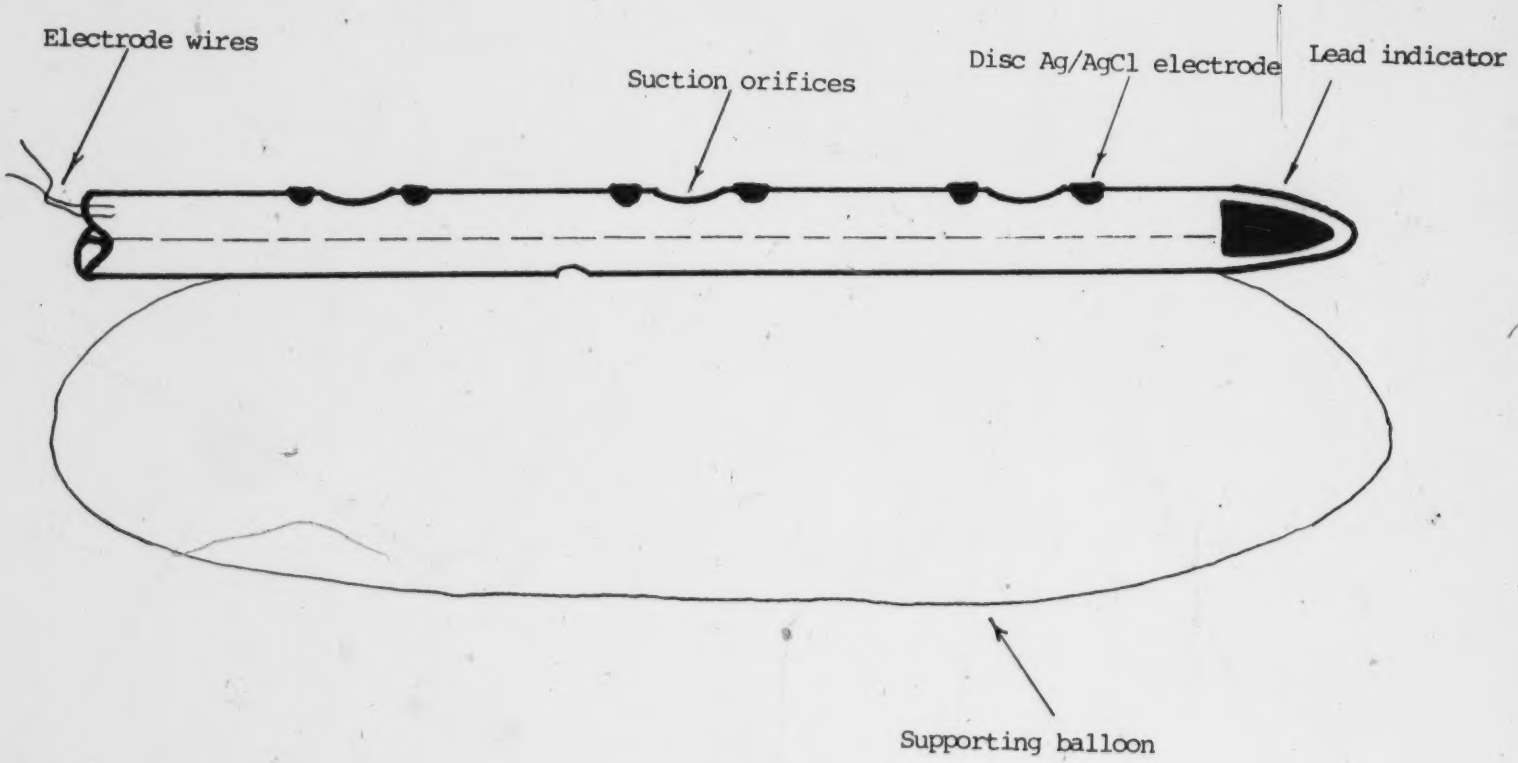

Figure 3.4 A schematic diagram of bipolar mucosal EGG suction electrode assembly II

(a) A double lumen nasal tube, gauge FR 14 is chosen as the assembly body.

(b) The top lumen as shown in Figure 3.4 is designed as a suction channel. Three suction orifices are located , 30 mm apart.

(c) Three pairs of Ag/AgCl disc electrodes are mounted on both sides of the suction orifices. The disc electrodes are 2.5 mm in diameter and their surfaces are polished , roughened and chlorided using the same procedure discussed in section 3.1. The purpose of disc Ag/AgCl electrodes is to increase the effective electrode area i.e. reduce electrode impedance in the low frequency range.

(d) A rubber balloon is mounted along the lower lumen of the nasal tube with an air orifice leading to the balloon. The balloon here functions to hold the electrodes against the stomach wall.

A sample of bipolar mucosal EGG recording from canine stomach is given in Figure 3.5. Trace A is respiration, trace B, C and D are mucosal EGG, where trace B is the most distal

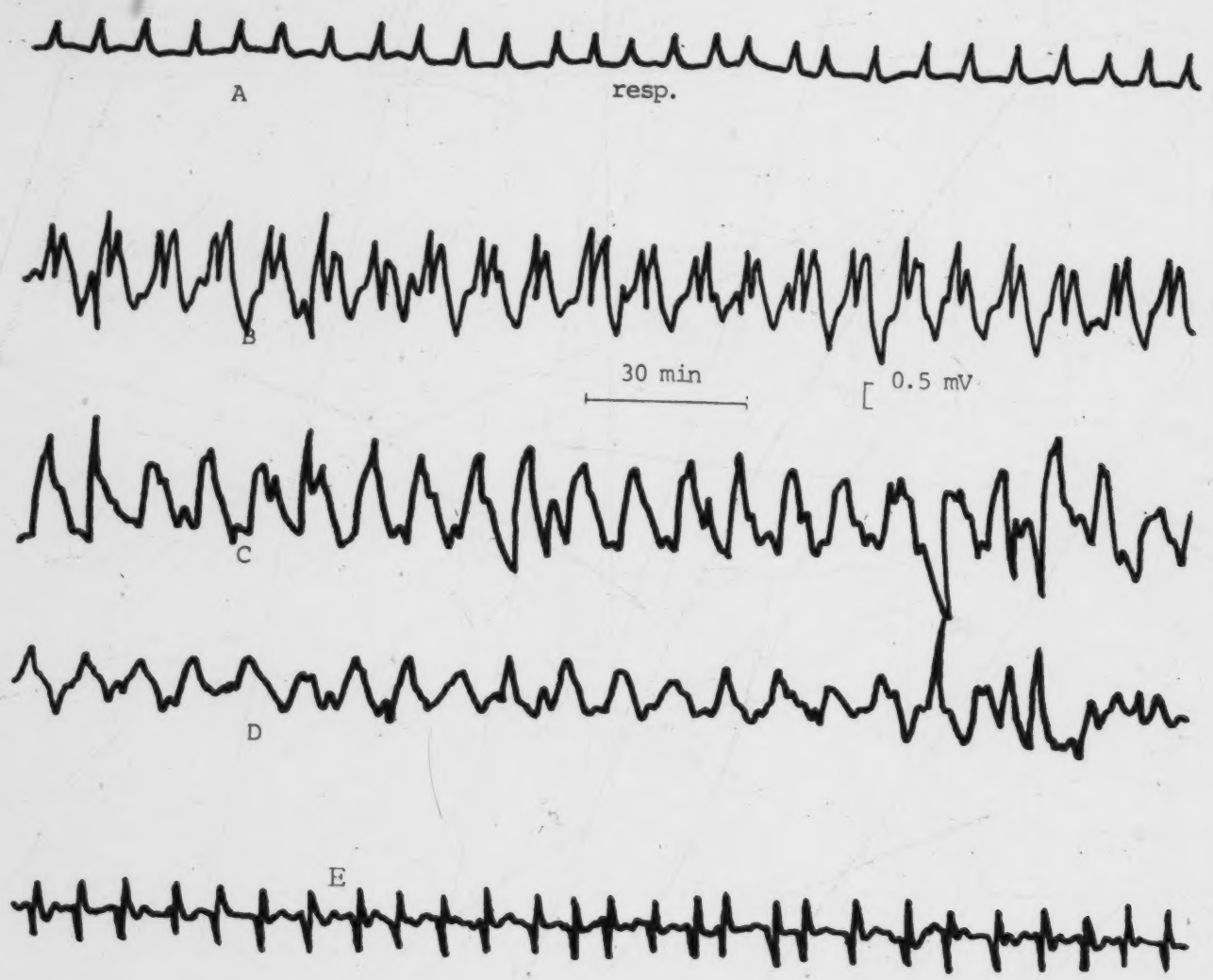

Figure 3.5 A canine mucosal EGG recording using suction electrode assembly II

electrode. Trace E is the pressure registered by the balloon. The mucosal EGG can be easily recorded using suction electrode assembly II on canine stomach, however, the poorer stability and the lack of long term high SNR are still a major problem. Since suction can sometimes cause partial mucosa-muscle separation, the validity of noninvasiveness is no longer applicable. In suction electrode assembly II, the supporting balloon can help the electrode to regain the proper suction on stomach wall. However, in the case that one or more suction orifices are blocked by mucosal debris regaining proper suction by a supporting balloon may fail. In general, the suction electrode assembly is applicable for the mucosal EGG recording, it still can not meet the requirements to be used as an ultimate mucosal EGG electrode. We shall search for a better method to record mucosal EGG.

3.3 RING ELECTRODE ASSEMBLY

The basic considerations for the design of the ring shaped electrode are based on:

(a) The reduction of electrode impedance is such that the low impedance artifact of gastric fluid can be reduced.

(b) The electrodes do not depend on the angular direction of the electrode contact with the stomach wall since ring electrodes have nearly 330 degree effective Ag/AgCl surface angle.

(c) The radial size of the assembly is reduced from 8mm to 5mm.

A schematic diagram of this type of electrode assembly is shown in Figure 3.6. The ring electrode assembly is based on a double lumen nasal tube. The electrodes are silver strips, 0.5 mm wide and 0.1 mm thick. they are mounted circularly on the tube. The distance between the electrodes is 20 mm for human stomach and 15 mm for canine stomach. In between the electrodes, three suction orifices are made. These suction orifices are designed to keep the electrode assembly in contact with the mucosa. As shown in Figure 3.6, a pressure sensing window is made between electrode 2 and 3 on the lower lumen

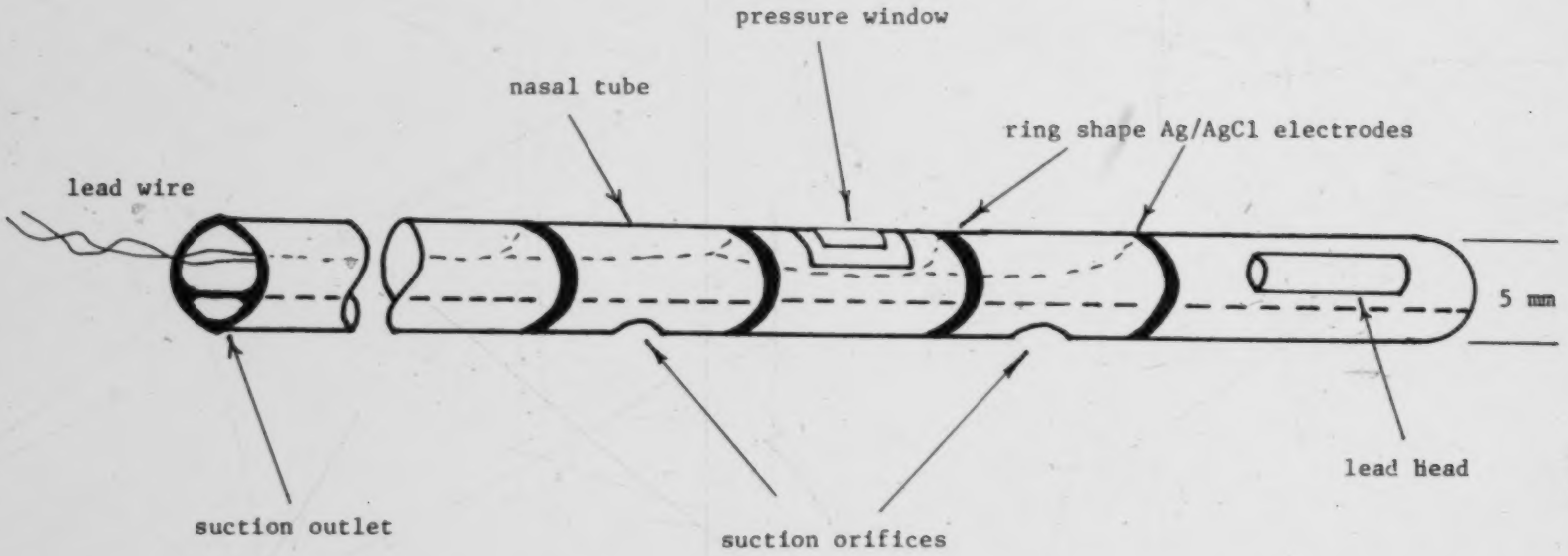

Figure 3.6 A schematic diagram of multichannel ring shape mucosal EGG electrode assembly

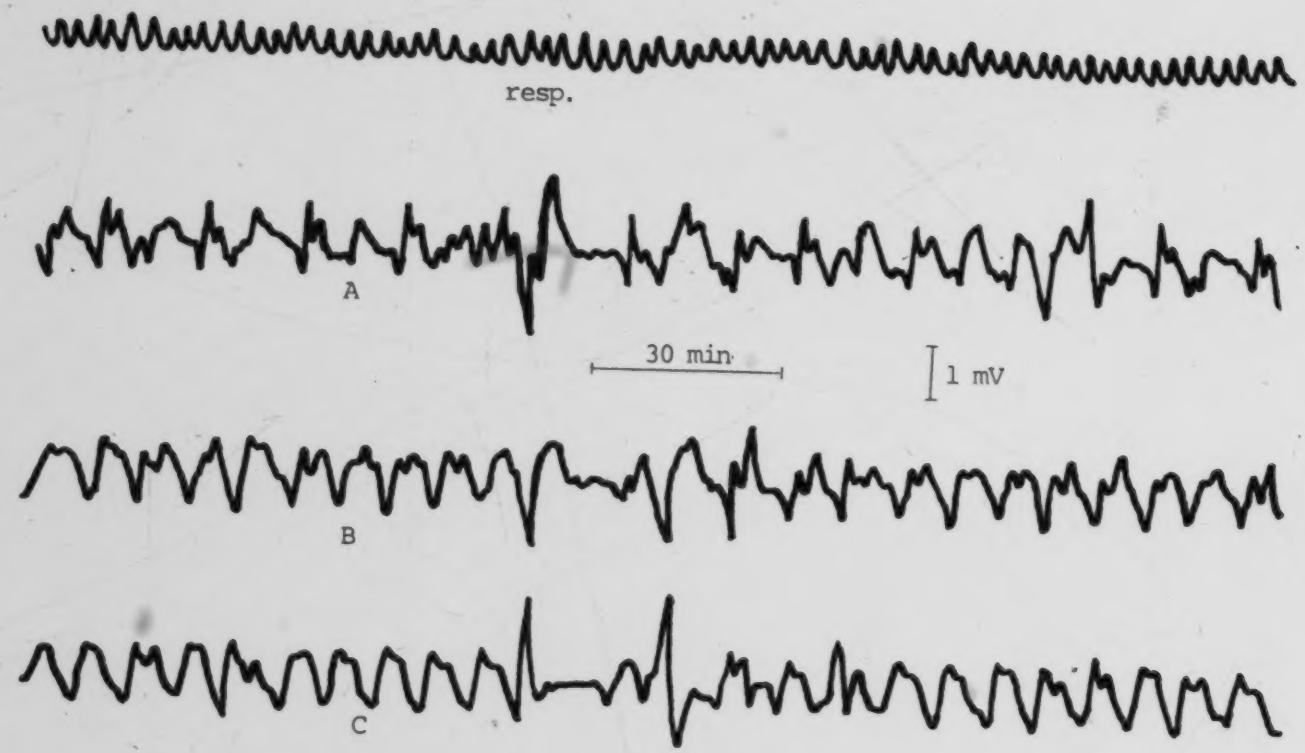

Figure 3.7 A canine mucosal EGG recording using ring electrode assembly

through which a pressure gauge is connected. This ring electrode assembly was applied to canine mucosa and a typical recording is given in Figure 3.7. Compared with the suction electrode assembly, the ring electrode assembly possesses the following advantages:

(a) The deterioration of the EGG signal caused by suction artifact can be avoided. Although there are one or more suction orifices between the ring electrodes, they serve only for electrode holding purposes. The separation of mucosal muscle would not have a strong impact on EGG recordings.

(b) electrode-mucosa contact does not depend on electrode angular orientation. The contact can be achieved by simply positioning the electrode along the antrum.

Some shortcomings were found during the experiments. Firstly, since the mucosal muscle becomes uneven when stomach muscle is contracted strongly, the ring electrode may ride on the top of the mucosal folds, so that poorer contact results. Secondly, the loss of holding suction also causes a electrode displacement from its initial position.

3.4 BALLOON ELECTRODE ASSEMBLY I

Balloon electrode assembly I, which is different from the suction electrode assembly, is based on the membrane self adhesion to hold electrodes onto the stomach mucosal wall. This surface adhesion is maintained by the existence of sufficient but not excessive gastric secretion in the membrane-mucosa interface. Two basic conditions are essential to ensure the wall contact:

(a) the rubber membrane on which the electrodes are mounted has to be very thin, which was about 30 micrometers in thickness in our experiment, so that the membrane can follow the contours of the uneven mucosa surface.

(b) the amount of gastric fluid in the membrane-mucosa interface should be adjustable. This is achieved by temporarily inflating the balloon and evacuating the excessive gastric fluid.

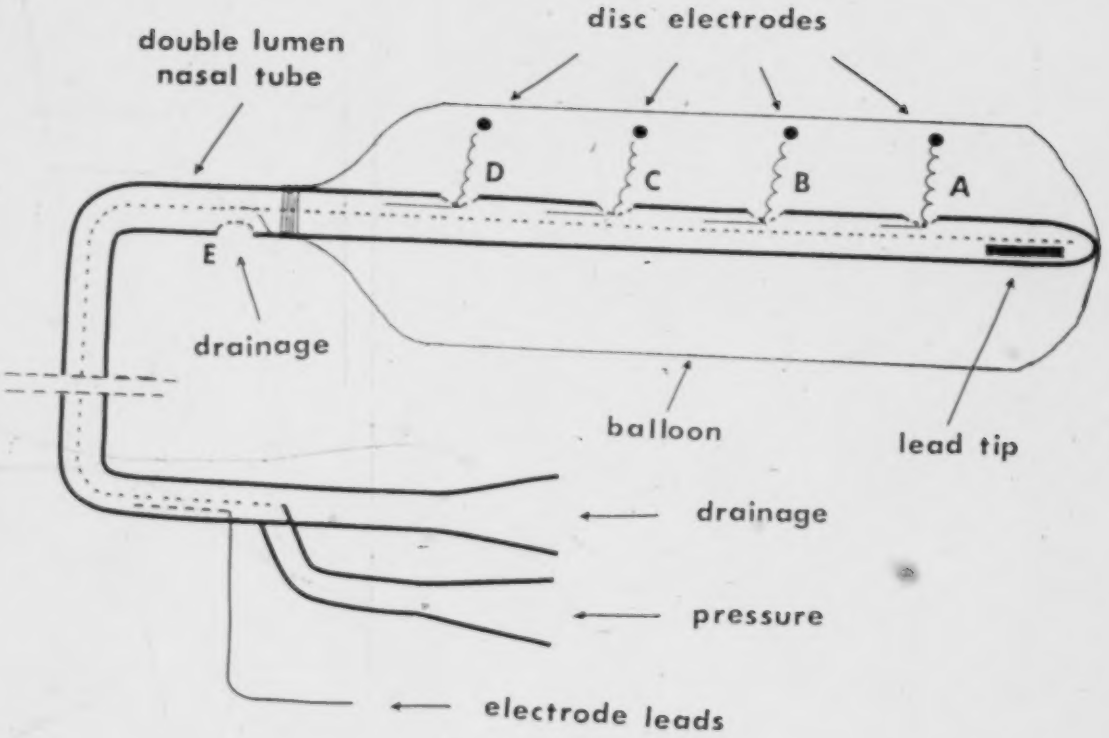

Figure 3.8 Balloon-shape gastric electrode assembly

Figure 3.8 presents a detailed structure of the balloon electrode assembly. A double lumen, gauge FR 14, nasal tube is used as the assembly body again. The head of the tube is redesigned as shown in Figure 3.8 so that a segment of lead bar, 10mm in length, 3mm in diameter is positioned inside the very end of the tube for fluoroscopic purposes. The tip of the tube is then sealed and smoothed by heating. There are four orifices, A, B, C and D, in the top lumen, 30, 45,60 and 75 mm apart for canine subject and 30, 50, 70 and 90 mm apart for human subject, from the end of the tube respectively. These four upper lumen orifices are designed correspondingly as gastric intraluminal pressure outlets; lead wire outlet and electrode shelters when suction is applied to hide the electrodes inside before the intubation. Higher up on the tube as shown in Figure 3.8, another two orifices, E and F, are located in the lower lumen. These are made for drainage or for possible medication and food ingestion. The disc electrodes discussed in the previous section are mounted on the surface of the thin rubber balloon as shown in Figure 3.8. In Figure 3.9 and 3.10, schematic diagrams are given to show the method to measure the surface adhesion force. From this configuration, we found that the typical adhesion peak appeared at the 1.5 mm membrane displacement. Figure 3.11 shows a diagram of mucosal EGG measurement system using balloon

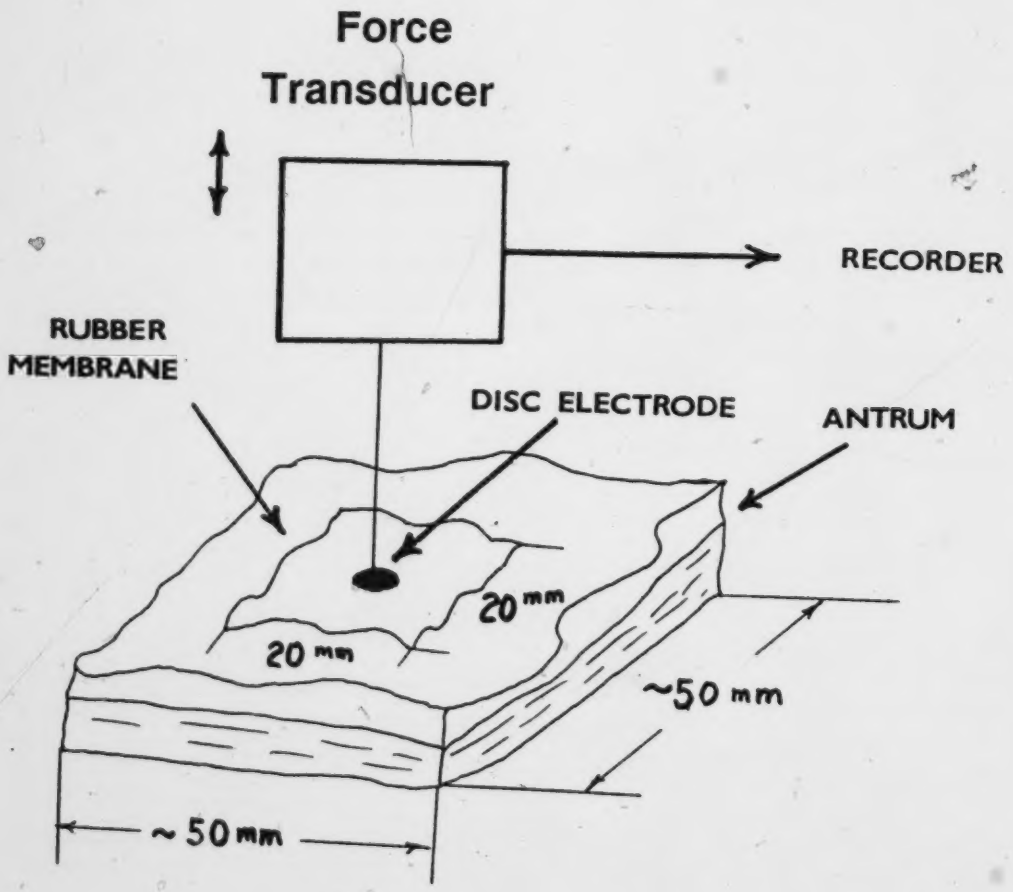

Figure 3.9 A schematic diagram of surface adhesion measurement

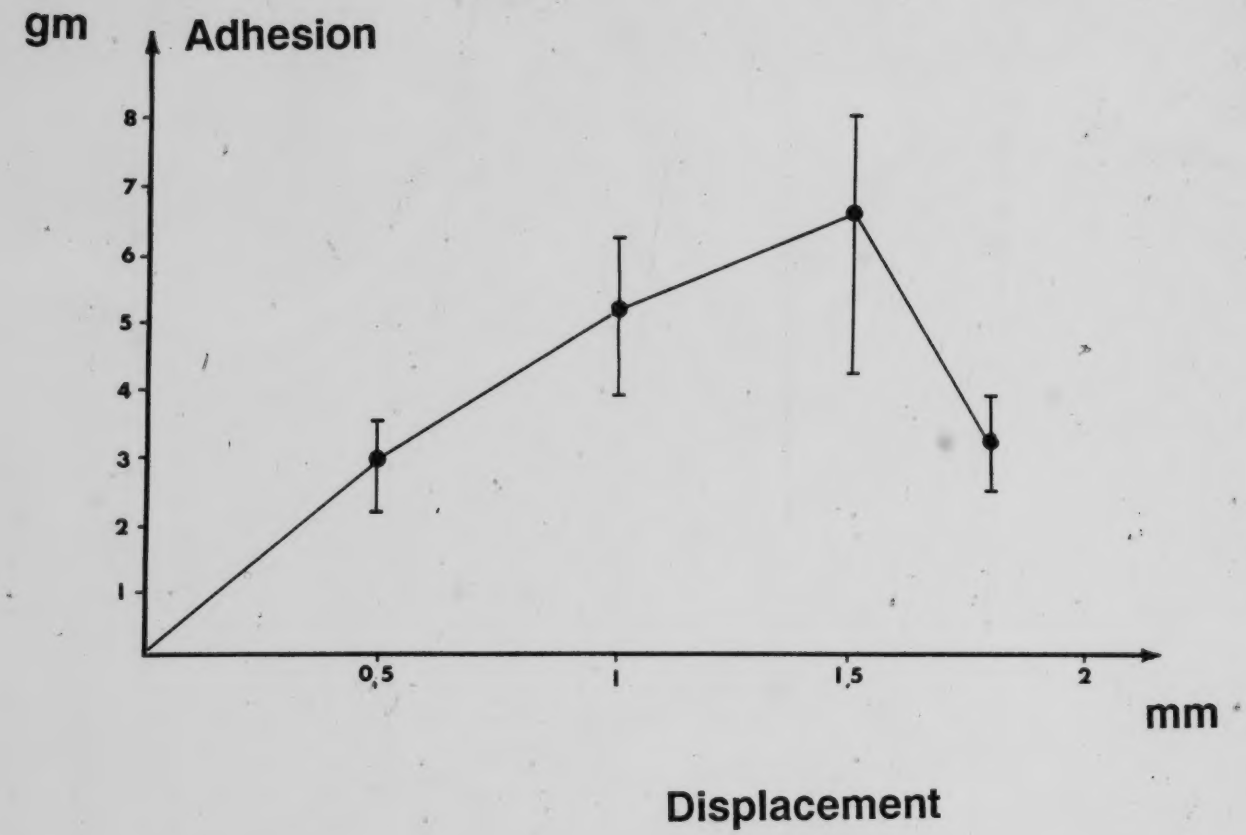

Figure 3.10 Surface adhesion vs electrode displacement

electrode assembly I.

A typical canine mucosal EGG recording using balloon electrode assembly I is given in Figure 3.12. Trace E is respiration, and trace A, B, C and D are monopolar EGG's, where trace D is the most distal electrode. From ten canine mucosal EGG measurements in-vivo, stable recordings were obtained for recording periods from 180 minutes to 360 minutes. Usually the signal shows larger amplitudes from the most distal electrodes. But this may not be always true since electrode-mucosa contact varies from one electrode to another, the waveforms may differ from one trace to another too. Using the balloon electrode assembly, the following improvements were obtained:

(a) The SNR has been increased and more discernible signal traces were obtained.

(b) Improved long term recording stability was achived. For an average of 240 minutes of recording time out of ten canine subjects, we were able to maintain a good signal quality.

(c) The previous suction and ring electrodes are susceptible to strong gastric contractions. An improvement in withstanding strong gastric contraction has been achieved using

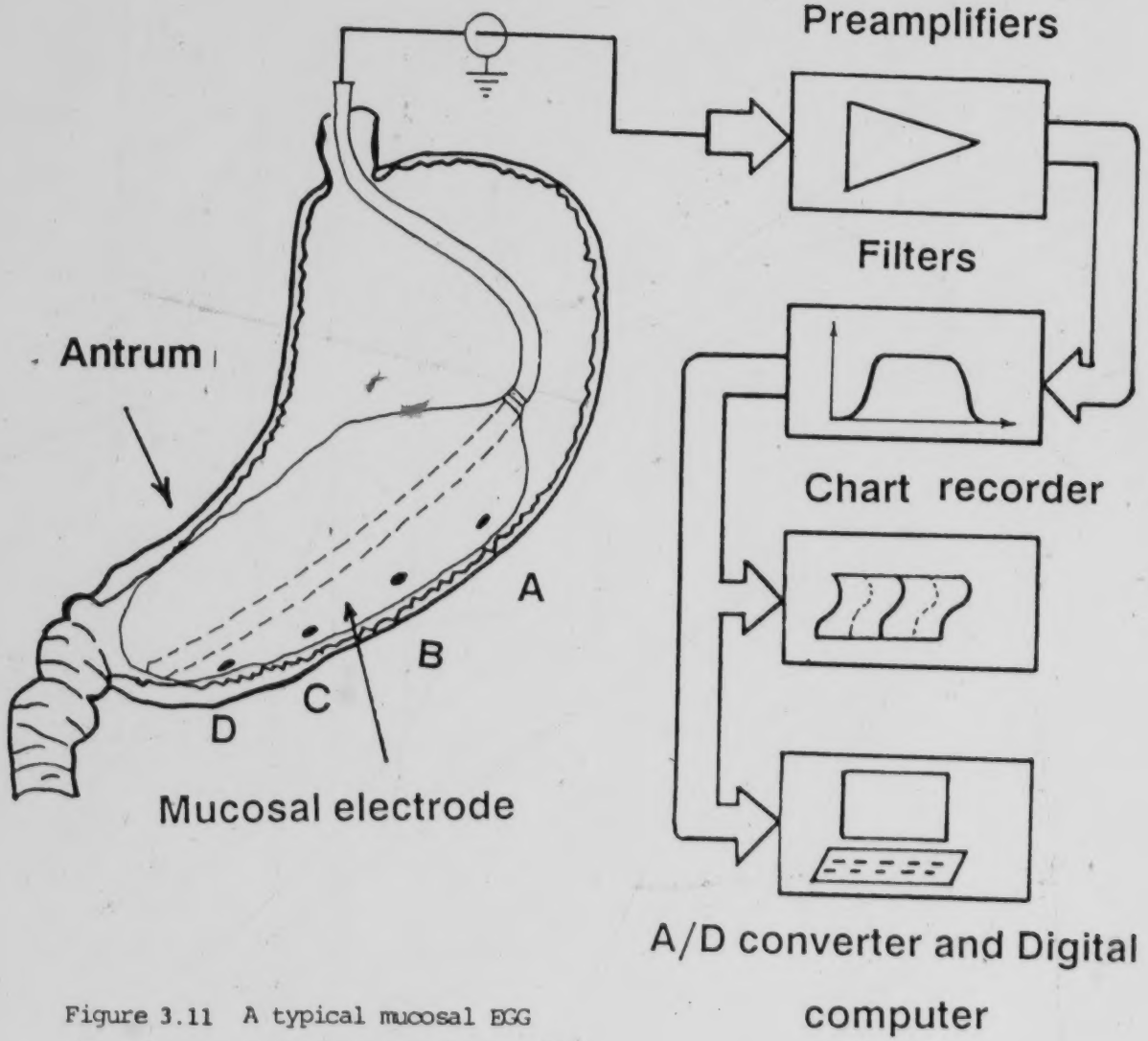

Figure 3.11 A typical mucosal EGG measurement system

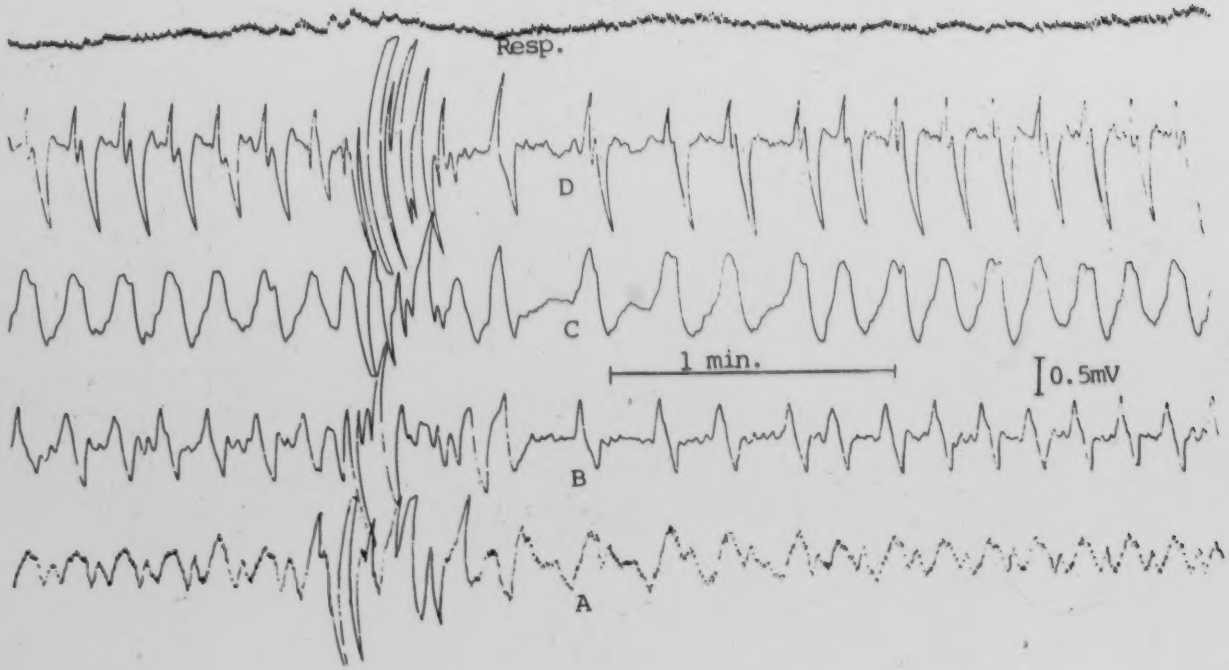

Figure 3.12 A canine mucosal EGG recording using balloon electrode assembly I

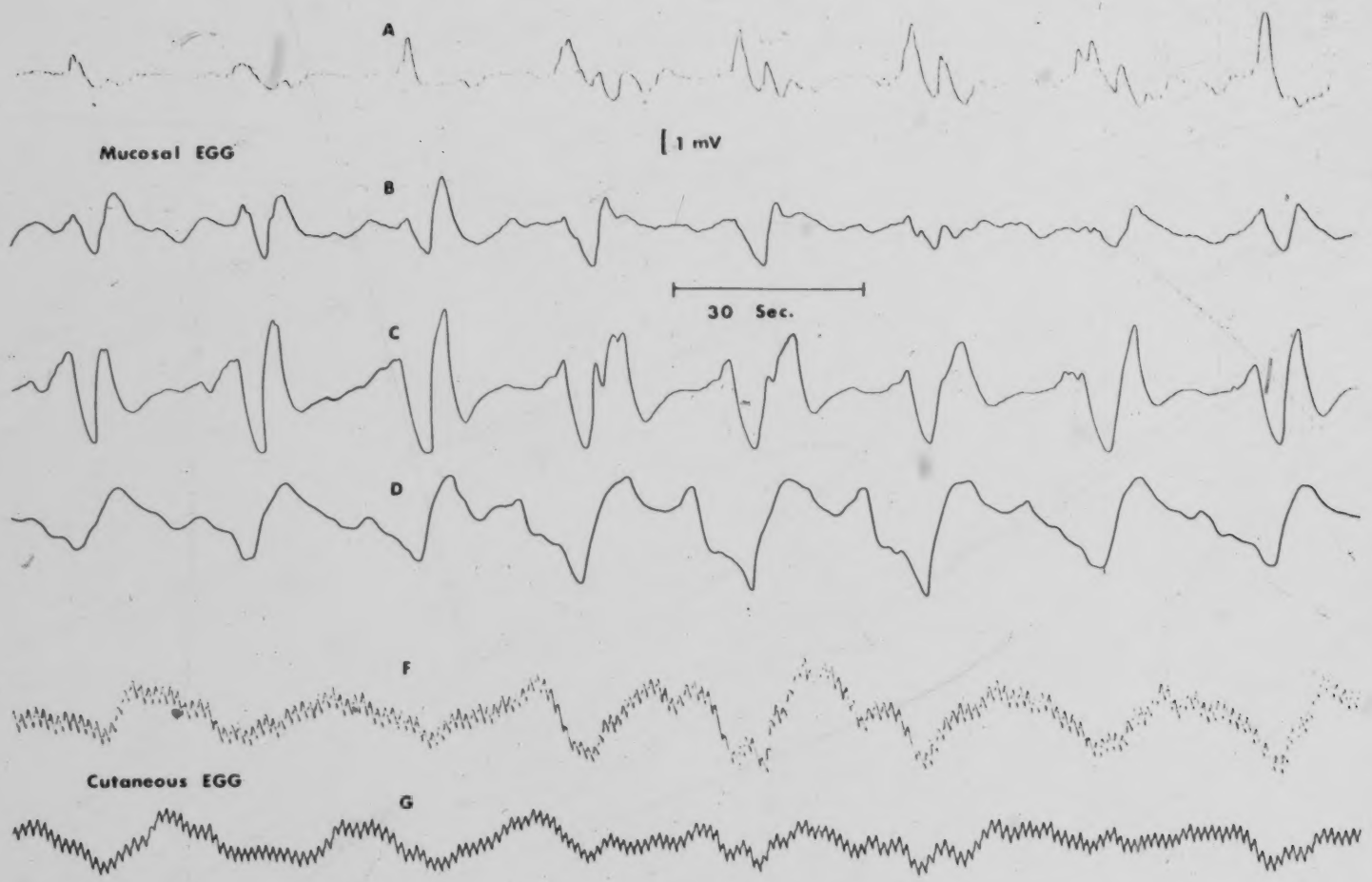

Figure3.13 A human mucosal and cutaneous EGG recording using balloon electrode assembly I

the balloon electrode assembly.

(d) unlike the suction and ring electrode assembly, the balloon electrode shows no damage on mucosal muscle.

After these successful experiments on canine stomach using the balloon electrode, we applied this type electrode on conscious human subjects. Figure 3.13 is a human mucosal EGG recording. Abnormal EGG propagation patterns were found in this recording. However, it was not easy to maintain a stable recording throughout the recording time on conscious human subject. The possible causes will be examined in the next section.

3.5 BALLOON ELECTRODE ASSEMBLY II

Using balloon electrode assembly I, a repeatable mucosal EGG recording was obtained in canine stomach. However, when we applied this electrode to human mucosal EGG recording, the stability and repetition were not satisfactory. The reasons are, perhaps that:

(a) the human antrum is larger than that of dog's. The balloon electrode, with only one available size, may not be able to effectively attach to the stomach wall, thus maximum adhesion can not be achieved.

(b) we tend to record human mucosal EGG from conscious subjects. However, gastric contractions are more vigorous in the conscious state than in the sedated state and the anesthesized state, consequently the electrode position in the antrum may change due to very strong gastric contractions and a poorer signal results.

(c) excessive gastric secretory fluid may cause the electrode assembly to float in the antrum and drift into other part of the stomach.

To correct the problems of balloon electrode I in human mucosal EGG recording, we designed a different type of balloon electrode assembly, which is shown in Figure 3.14. There are three balloons mounted on the nasal tube and the following considerations were taken into account:

(a) balloon A is of the normal size, 40 mm non-stretched

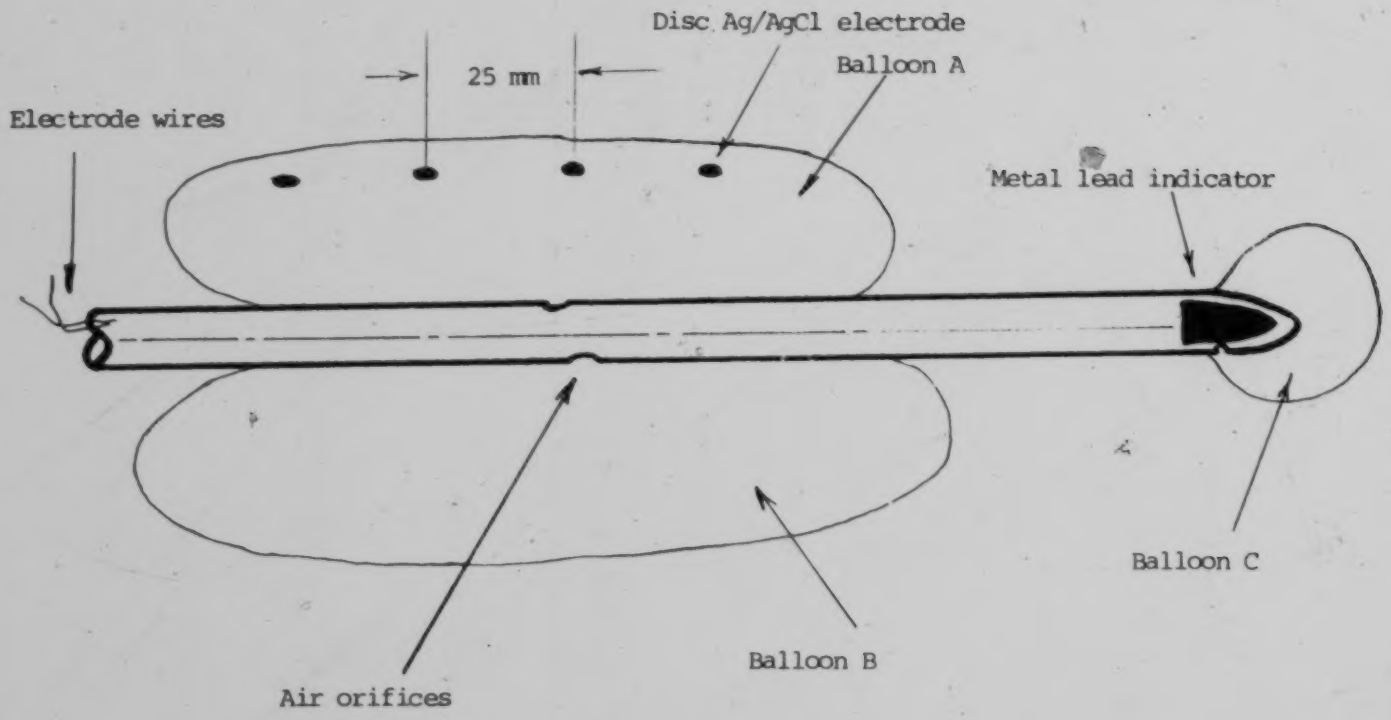

Figure 3.14 A schematic diagram of balloon electrode assembly II

diameter. Four disc Ag/AgCl electrodes are glued on the surface of balloon A and the electrode wires are threaded through the upper lumen. Then balloon A , 40 mm away from the tube end , is glued along the upper lumen with an air outlet to the balloon. A supporting balloon B is mounted along the lower lumen opposite from balloon A. The effective non-stretch assembly radial size increases from 40 mm to about 85 mm.

(b) the double balloon structure can make an air way in antrum, which in turn the effect of gastric contraction may be reduced.

(c) balloon C is mounted on the tip of the tube as shown in Figure 21. It functions as a trapping balloon which is passed through the pylorus and positioned in the duodenum before inflating it. As balloon C is trapped in the duodenum , balloon A and B will be kept in the terminal antrum. We have applied this type of electrode to two human subjects, the preliminary results are encouraging. Figure 3.15 gives a sample of human mucosal EGG.

Figure 3.15 A human mucosal BGG using balloon electrode assembly II

3.6 CLIP MUCOSAL EGG ELECTRODE

The detachable biopsy clip technique has been used in gastrointestinal research and clinical applications for many years. However, applying clip electrodes for mucosal EGG measurement has not been reported. In our research, we have successfully applied the clip electrode in canine mucosal EGG recordings. The design of the clip mucosal EGG electrode was motivated by:

(a) the fact that the biopsy clip is made of stainless steel. It is known that the stainless steel is also a good bioelectrode metal. If the low impedance gastric secretory fluid would not be a major artifact, we can directly apply the detachable biopsy clip to the gastric mucosal wall and record the EGG signal.

(b) a report by Mclauchlan [33] that the properly applied biopsy clip can reach the submucosal layer where a better EGG signal to noise ratio is expected.

(c) the fact that using a wide channel gastric endoscope, multichannel clip electrodes can be positioned in a single

intubation. After the electrodes have been clipped onto the mucosal wall, the endscope can be withdrawn and only several very fine lead wires remain in the throat. In Figure 3.16 the schematic diagram is given to show how the clips work.

A mucosal EGG recording using two clip electrodes on canine stomach is given in Figure 3.17. The clip electrodes were positioned in canine terminal antrum, 70 mm and 20 mm to the pylorus respectively. Electrode B is the most distal electrode. The signal amplitude is about 0.4 mV per cm. We concluded from the experiment that the clip electrode technique has the following advantages:

(a) By employing a wide channel endoscope, multi-electrode measurement can be performed. After the electrodes are positioned, the endoscope can be removed and only electrodes and lead wires remain in the stomach.

(b) unlike the balloon electrode assembly, the stomach remains in nonstretched state, we assume that the mucosal EGG is least disturbed.

(c) it is made possible to allow feeding and intake of medicine during the mucosal EGG measurement.

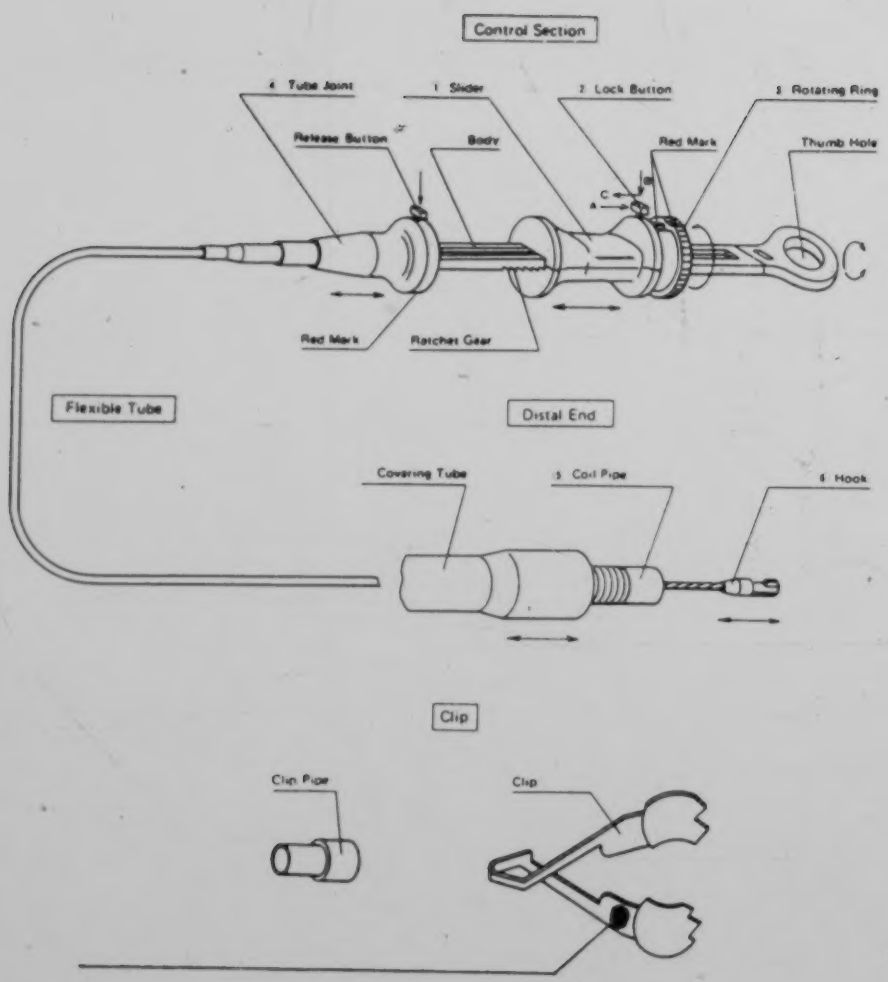

Figure 3.16 The clip setter used in positioning clips on antrum mucosal muscle through endscope

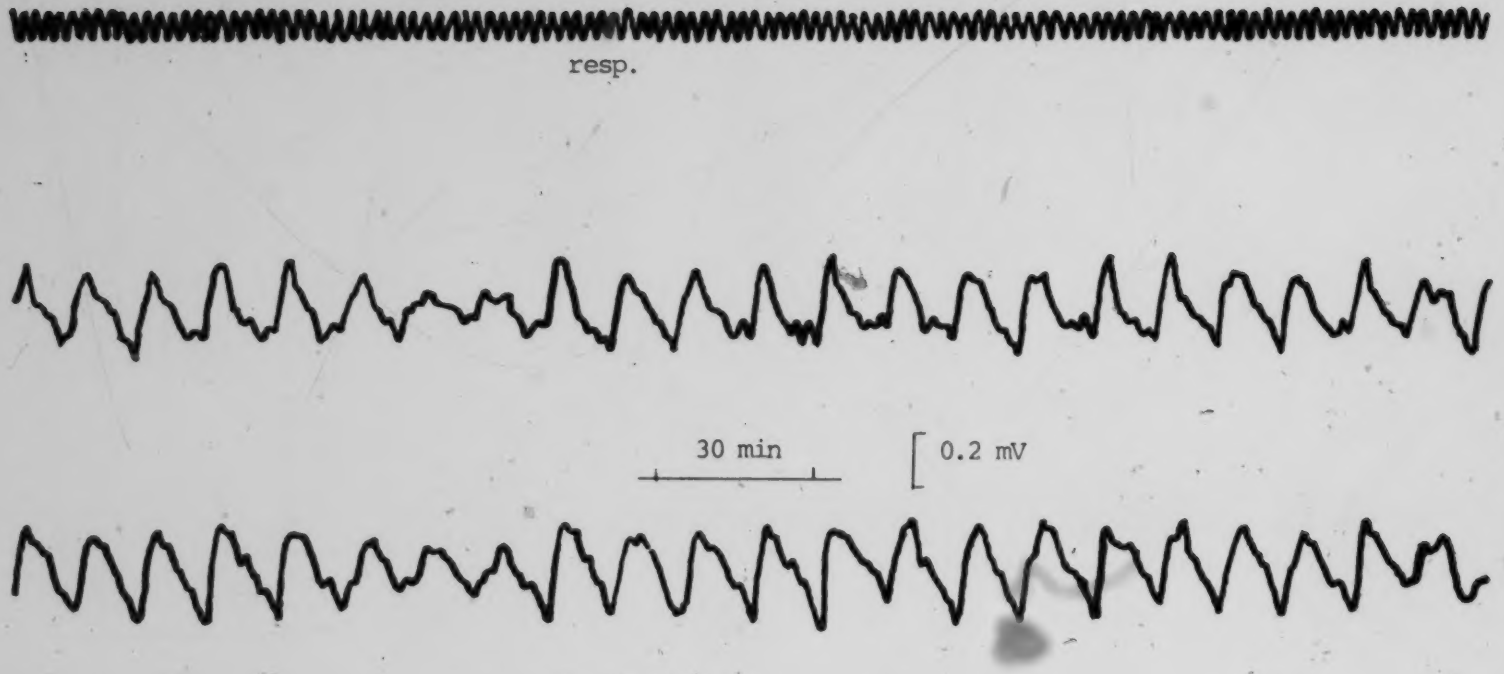

Figure 3.17 A canine mucosal EGG using clip electrode

(d) the electrode structure is simple and easy to manufacture, thus very low cost is expected for the clip electrode.

3.7 SUMMARY OF CHAPTER 3

In this chapter, a mumber of mucosal gastric electrodes were discussed. The design of those electrodes were given and the experiments on canine and human stomach were reported using those electrodes. In our experiments, we found that the suction electrodes ofter suffer a low SNR and very short measurement time; The ring-shaped electrode assembly is the most compact one. Its large effective electrode area may provide certain improvement on SNR. But maintaining a good electrode-mucosal contact is still an unsolved problem; The balloon electrode assembly is proven to have more tolerance to strong gastric contraction; Finally, the clip electrode has been tested on canine stomach and good canine EGG recordings suggest that the clip electrode can provide an alternative method to measure gastric electrical activity. In the next chapter, we will discuss a study on the measurements of the magnetic field in intact gastric canine antrum.

CHAPTER 4

A STUDY OF THE MEASUREMENT OF MAGNETIC FIELDS IN INTACT ANTRUM

4.1 INTRODUCTION

Although the electrical potentials produced by gastric smooth muscle in the antrum can be readily measured, and the temporal and spatial characteristics of gastric electrical events are well understood, the accompanying magnetic field of the antrum both in human and animal have so far never been studied.

Over the last several years, volume conductor models developed in the 1960's have been used to describe electrically active tissue such as nerve axons [21-26], nerve bundles[28], cardiac muscle [5] and gastric smooth muscle [4-6]. The primary purpose of these models has been to relate extracellular and transmembrane potentials [11,17]. As a theoretical background, the volume conductor models have also been applied to calculate the magnetic fields produced by the moving dipoles along the nerve axons and certain orientations in muscle strands [20-26,29]. The significance of the

magnetic field is that the distribution of action current can be directly related to the magnetic fields [28].

It is well known that the ECA in the antrum can be modeled as a dipole band moving distally[17], and the corresponding intracellular and muscle surface potentials are readily obtainable. It is possible, therefore, to calculate the accompanying magnetic field using a volume conductor model.

In this chapter, the discussion will be focused on the necessary theoretical fundamentals of magnetic fields associated with gastric electrical activity using volume conductor models. As well, we will examine the validity of our experiments performed in-vivo and in-vitro in attempting to measure magnetic fields on the internal and the external surfaces of antral muscle wall. The potential advantages of magnetic field measurements are:

(a) since the strength of magnetic fields is closely related to the stregth of current density in the muscle, the current distribution patterns in antrum can be revealed by the interpretation of measured magnetic fields.

(b) the magnetic fields can be measured without physical

contact with the sample tissue. Thus noninvasive measurements can be performed.

(c) the magnetic fields on the muscle surface decay cubically proportional to the increase of the distance. The contributions of magnetic fields from other organs may be negligible.

4.2 A STUDY OF EXTRACELLULAR POTENTIAL AND MAGNETIC FIELDS OF ANTRUM SMOOTH MUSCLE: A FORWARD PROBLEM

1. THE POTENTIALS

To calculate the internal and external potential in antrum, we may simulate the antrum by a long cylindrical object of radius a, with finite wall thickness δ, separating the internal and external media. Figure 4.1 shows a schematic configuration of this simulation. We first assume that the media inside and outside the muscle wall have homogeneous, isotropic conductivities σ_i and σ_e, respectively. As shown in Figure 4.1, the cylindrical coordinates ρ, θ and z are specified as radial, azimuthal, and axial positions. One simplification is made in this simulation. Since $a \gg \delta$, where the average value of a is about 40 mm and the average δ is about 4 mm, thus, the muscle wall thickness is assumed to be negligible. Plonsey[20] has shown that if we assume quasi-stationarity for this system, then Laplace's equation is satisfied for internal and external media. That is, at an

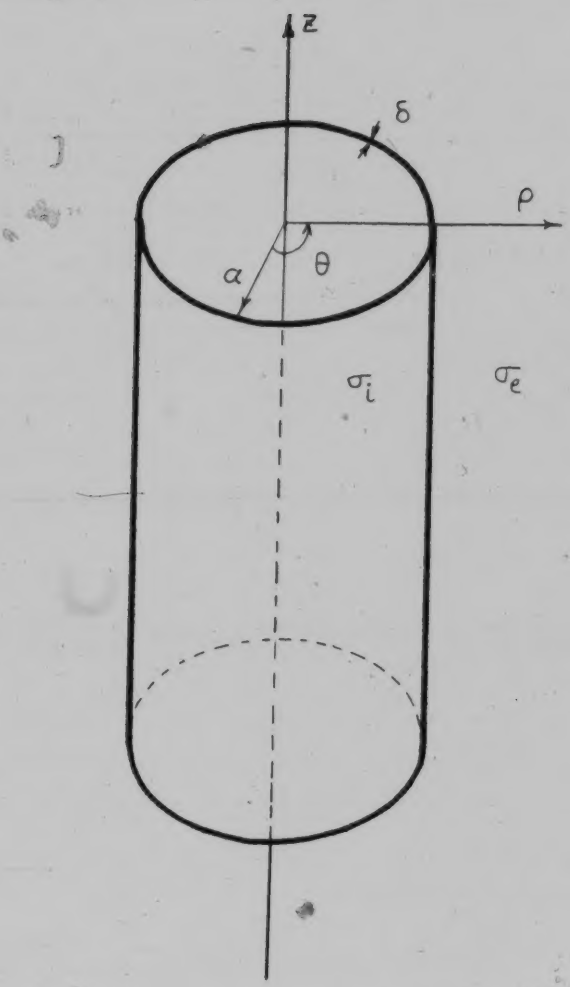

Figure 4.1 The antrum is simulated by a long cylindrical object immersed in the internal and external media with conductivity σ_i and σ_e, respectively

arbitrary point in the external medium, the potential is expressed as:

$$\nabla^2 \Phi (\rho , \theta, z) = 0 \qquad \rho > a \qquad \text{-4.1-}$$

and in the internal medium:

$$\nabla^2 \Phi (\rho, \theta, z) = 0 \qquad \rho < a \qquad \text{-4.2-}$$

For negligible muscle wall thickness, the internal and external current density, I_i and I_e obey the continuity condition[23]:

$$I_i = - I_e \qquad \text{-4.3-}$$

Given the muscle wall potential, the solution of Laplace's equation, 4.1 and 4.2 can be obtained by the

separation of variables of the Laplace's equation in cylindrical coordinates. The form of the solution for the external medium is[26] :

$$A(k)\ K_o(k\ \rho)\ e^{jkz} + B\ (k)\ K_o(k\ \rho)\ e^{-jkz} \qquad -4.4-$$

where K is the modified Bessel function of the second kind. The most general form can be written as:

$$\Phi_e(\rho,z\ ) = \int_0^\infty [A(k)\ K_o(k\ \rho)e^{\ jkz} + \int_0^\infty B(k)K_o(k\rho)e^{-jkz}]dk$$

-4.5-

Thus, a more compact form is [20]:

$$\Phi_e(\rho,z) = \frac{1}{2\pi}\int_{-\infty}^{\infty} C(k)K_o(|k|\rho)\, e^{-jkz}dk \qquad -4.6-$$

where

$$\frac{C(k)}{2\pi} = B(k) \qquad \infty > k > 0$$

$$= A(-k) \qquad 0 > k > -\infty$$

The function C(k) can now be described in terms of the given potential boundary condition:

$$\Phi_1(z) = \Phi_e(a,z) \qquad -4.7-$$

Then we have:

$$\Phi_e(z) = \frac{1}{2\pi}\int_{-\infty}^{\infty} C(k)\, K_o(|k|a)\, e^{-jkz}dk \qquad -4.8-$$

By taking the inverse transform we get:

$$C(k)K_o(|k|a) = \int_{-\infty}^{\infty} \Phi_e(z)\, e^{jkz} dz = F_e(k) \qquad -4.9-$$

and

$$C(k) = \frac{F_e(z)}{K_o(|k|a)}$$

Finally, the potential anywhere in the external medium is expressed as [21]:

$$\Phi_e(\rho,z) = \frac{1}{2\pi} \int_{-\infty}^{\infty} \frac{F_e(k)K_o(|k|\rho)}{K_o(|K|a)}\, e^{-jkz}\, dk \qquad -4.10-$$

By applying the same procedure, the potential anywhere the internal medium is found:

$$\Phi_i(\rho,z) = \frac{1}{2\pi}\int_{-\infty}^{\infty} \frac{F_i(k)I_o(|k|\rho)}{I_o(|k|a)} e^{-jkz}\,dk \qquad \text{-4.11-}$$

where I_o is the modified Bessel function of the first kind.

It was shown[24] that equation 4.11 can be further developed into a more explicit form by directly relating the muscle wall potential $\Phi_m(z)$ to the external and internal potentials. To achieve this, we first find the relation between $F_e(k)$ and $\Phi_m(k)$:

$$F_e(k) = \frac{\phi_m(k)}{\alpha(|k|a)} \qquad \text{-4.12-}$$

where

$$\alpha(|k|a) = \frac{\sigma_e K_1(|k|a)I_0(|k|a)}{\sigma_i K_0(|k|a)I_1(|k|a)} - 1$$

By substituting equation 4.1 into equation 4.10, one obtains a potential at an arbitrary point anywhere in the external medium of the antrum [20]:

$$\Phi_e(\rho,z) = \frac{1}{2\pi}\int_{-\infty}^{\infty} \frac{K_0(|k|\rho)}{\alpha(|k|a)K_0(|k|a)} \Phi_m(k)e^{-jkz}dk$$

-4.13-

and by similar operation, the potential anywhere in the internal medium is:

$$\Phi_i(\rho,z) = \frac{1}{2\pi}\int_{-\infty}^{\infty} \frac{I_0(|k|\rho)}{\beta(|k|a)I_0(|k|a)} \Phi_m(k)\, e^{-jkz}\, dk$$

-4.14-

where

$$\alpha(|k|a) = -(1 + \gamma(|k|a))$$

$$\beta(|k|a) = 1 + \frac{1}{\gamma(|k|a)} \qquad \text{-4.15-}$$

with γ given by

$$\gamma(|k|a) = \frac{\sigma_e K_1(|k|a) I_0(|k|a)}{\sigma_i K_0(|k|a) I_1(|k|a)} \qquad \text{-4.16-}$$

4.2 MAGNETIC FIELDS

To calculate the associated magnetic field given the muscle wall potential, both Ampere's Law and the Law of Biot and Savart can be applied[26]. Mathematically, the difference in the two approaches is that with the Law of Biot and Savart, the radial integration of the current density is implicit and only the axial integration must be performed explicitly. While with Ampere's Law the axial integration of the current density is implicit and only the radial integration must be performed[27].

Since the calculation of the associated magnetic fields using the Law of Biot and Savart is quite tedious, we will discuss here the approach using Ampere's Law only.

Ampere's Law states that:

$$\oint_c \underline{B} \cdot d\underline{l} = \mu_0 I_{enclosed} \qquad -4.17-$$

Where $I_{enclosd}$ is the net current threading the closed path

c, and μ_o is the permeability of free space, $4\pi \times 10^{-7}$ TmA.$^{-1}$

Noting the cylindrical symmetry, we can simplify equation 4.17 into:

$$2 \pi \rho B(\rho, z) = \mu_0 I_{enclosed} \qquad -4.18-$$

where the path of integration is a circle of radius centered at z, and $I_{enclosed}$ is the sum of the total current in the internal current $I_i(z)$ and external current $I_o(\rho,z)$. Here we assume that only the internal current has axial current.

By using the two Bessel function relationships [27]:

$$\int x I_0 (x)\, dx = x I_1 (x) \qquad -4.19-$$

and

$$\int x K_0 (x)\, dx = - x K_1(x) \qquad -4.20-$$

and denoting the Fourier transforms of $I_i(z)$ and $I_e(\rho,z)$ as $I_i(k)$ and $I_e(\rho,k)$, we can perform the integration to find:

$$I_i(k) = \frac{2\pi\sigma_i ik}{\beta(|k|a)I_0(|k|a)|k|} aI_1(|k|a)\ \Phi_m(k)$$

-4.21-

and

$$I_e(\rho,k) = \frac{2\pi\sigma_e ik}{\alpha(|k|a)K_0(|k|a)|k|} \{aK_1(|k|a) - \rho K_1(|k|\rho)\}\ \Phi_m(k)$$

-4.22-

Then the corresponding magnetic fields have the Fourier transform:

$$B_i(\rho,k) = \frac{\mu_0\sigma_i ik}{\rho\beta(|k|a)I_0(|k|a)|k|} aI_1(|k|a)\ \Phi_m(k)$$

-4.23-

and

$$B_{\bullet}(\rho,k) = \frac{\mu_0 \sigma_{\bullet} ik}{\rho\alpha(|k|a)K_0(|k|a)|k|} \{aK_1(|k|a) - \rho K_1(|k|\rho)\}\ \Phi_m(k)$$

-4.24-

The final step is to add these two contributions to give a equation which relates the magnetic field to the muscle wall potential:

$$\overline{B(\rho,k)} = \frac{i\mu_0 k}{\rho|k|} \left\{ \frac{\sigma_i \alpha I_1(|k|a)}{\beta(|k|a)I_0(|k|a)} + \frac{\sigma_{\bullet}}{\alpha(|k|a)K_0(|k|a)} \right.$$

$$\left. \overline{[aK_1(|k|a) - \rho K_1(|k|\rho)]} \right\} \Phi_m(k) \qquad \text{-4.25-}$$

Five parameters are required by the volume conductor model:

1) the conductivity of the external medium σ_e.

2) the conductivity of the internal medium σ_i.

3) ECA propagation velocity u.

4) the antrum radial size a.

5) the field point radius ρ.

The dependence of equation 4.23 and 4.24 on these parameters is quite complex. We should note that in this model, we have assumed that the antrum wall thickness is negligible if we measure the magnetic field anywhere from the muscle surface. In fact, the antrum wall has finite thickness, the antrum radial size should be considered to be the average radial figure. Thus, if we assign ρ on the muscle surface, the second term of the resultant magnetic field $B(\rho,z)$ in equation 4.25 will not vanish since $\rho \neq a$.

Equation 4.25 also tells us that the magnetic field is proportional to the spatial frequency k, the strength of muscle surface potential $\Phi_m(k)$, internal conductivity σ_i and external conductivity σ_e.

4.3 A TENTATIVE DIRECT MEASUREMENT OF MAGNETOGASTROGRAM(MGG) IN CANINE ANTRUM

We have designed an experiment to directly measure the magnetic field on the internal and external surface of the stomach in canine. It is known that the gastric electrical activity presents itself in the form of slow waves which are the consequences of millions of cells depolarized as a narrow dipole band in the antrum muscle, propagating distally to the pylorus. The slow wave repeats itself with a period of 10 to 15 seconds in canine stomach and 20 seconds in human stomach. The current density distribution associated with the dipole band will be present in the internal medium and external medium of the antrum. A schematic diagram showing the current density distribution in antrum is given in Figure 4.2. The orientations of the associated magnetic fields are parallel to the orientation of circular muscle as shown in Figure 4.2. In canine stomach, the slow wave potential contains mainly low frequency components, approximately from 0.013 to 0.1 Hz.

Therefore the measurement system is required to have a linear bandwidth from DC to 0.5 Hz. Currently, the SQUID (superconducting quantum interference device), has been

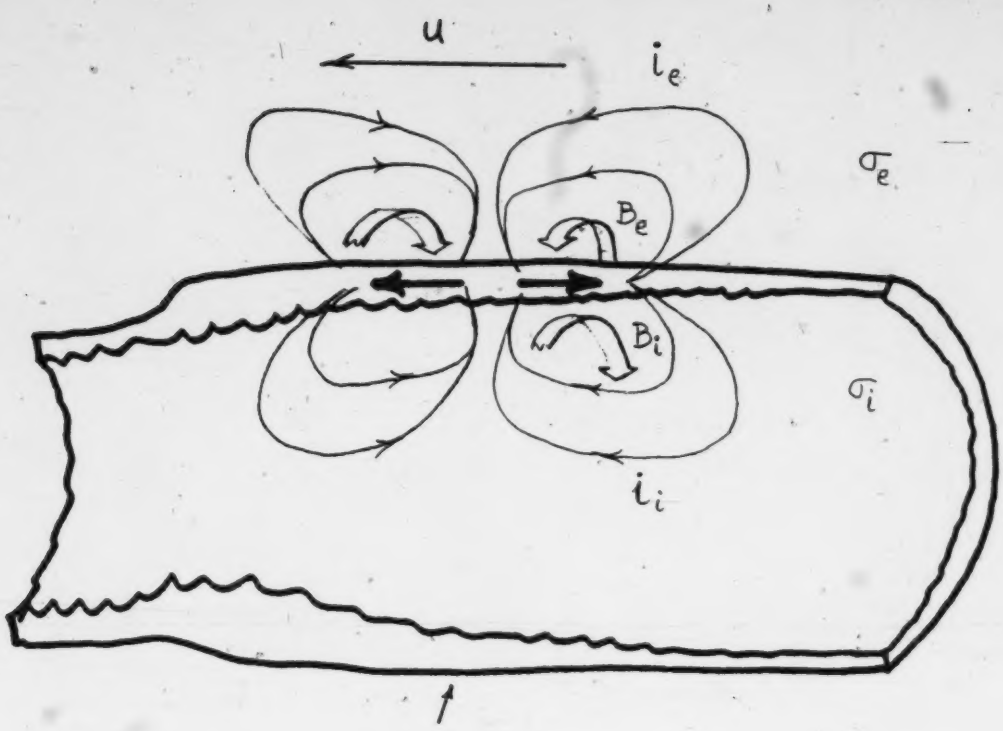

Figure 4.2 A schematic diagram showing the moving dipole band, current density and associated magnetic fields

used [16] to measure biomagnetic fields. It can provide a bandwidth of 0.01 Hz to 1 kHz with a sensitivity of 0.01 pTesla of change in magnetic flux through a superconductive pick up coil[15].

Due to unavailability of a SQUID, an alternative approach of using a Gaussmeter with a Hall effect transducer may be applicable to the MGG measurement.

With proper filters and amplifiers, the discernible sensitivity of this measurement system can be as high as 10 nTesla. There are two kinds of Hall effect transducers available at this moment. One is the cylindrical Hall effect transducer which only senses axial orientation flux. The second is a narrow flat sheet type of Hall effect transducer which senses magnetic fields perpendicular to its surface. Since the flat Hall effect transducer has a larger area, it can provide 5 to 10 times higher sensitivity than that of the cylindrical transducer. To remove high frequency artifact and system DC drift, a band pass filter was chosen with a bandwidth of 0.013 to 0.8 Hz. The noise level which will eventually limit the sensitivity of the measuring system may be attributed to the transducers' thermal noise, background magnetic noise and circuit noise. The analog band pass filter is ineffective to reduce this random noise. Signal averaging

techniques can be used in this case[15].

Since exact MGG patterns and signal strength in canine antrum are unknown at this moment, our model can be applied to predict the resultant MGG. We may assume that the major contributions of a moving dipole band to the magnetic field are circularly oriented as shown in Figure 4.2. However, the nonisotropic properties of ECA in circular orientation from exterior side to interior side of the antrum may also produce a magnetic field that differs from that of the distally moving dipole band.

In our experiments, we performed mucosal MGG measurements and serosal MGG measurements. In each of these experiments, the magnetic field components along the circular orientation and the longitudinal orientation were measured separately with the Hall effect transducer specifically sensitive to that particular orientation of magnetic field component.

4.4 MUCOSAL MGG MEASUREMENT

This experiment was conducted on the stomach of anesthetized dog. A one inch incision was made on the mid fundus. The transducer was placed in the antrum through the incision. As shown in figure 4.3, the transducer sensing surface was positioned perpendicular to the assumed magnetic flux adjacent to the mucosal wall. To reduce thermal disturbance and gastric fluid artifact, the transducer was mounted in a plastic tube and fixed on a rigid brass rod. The sensitivity on the Gaussmeter is 1 μTesla per division, and the sensitivity on the Beckman chart recorder was set to 0.1 mV per cm. The system provided approximately 10 nTesla discernible flux sensitivity. A bandwidth of 0.013 to 0.8 Hz was chosen for the band pass filter to reduce DC drift and frequencies above 1 Hz.

It is noticed that motion of the intact stomach caused by respiration may cause a very strong artifact due to the existence of a constant earth magnetic field. To reduce this type of artifact, a pair of cancellation coils were designed . The dimensions of square shaped cancellation coils were chosen to be 300 mm wide and 300 mm long, with a total of 200 turns. With two coils, parallel, 250 mm apart, the cancellation effect

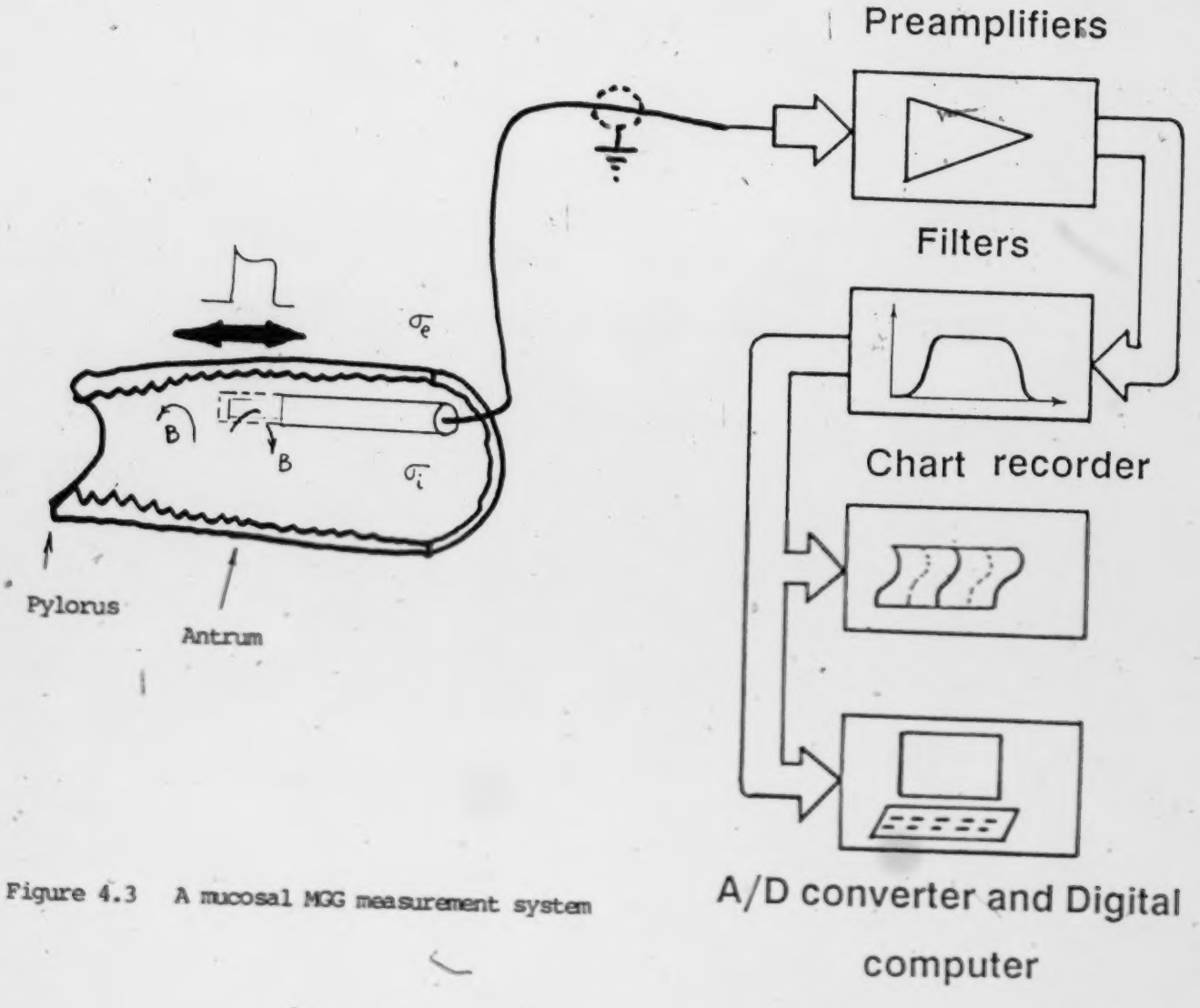

Figure 4.3 A mucosal MGG measurement system

is achieved at the central area by applying 80 mA DC current to the coils. Without cancellation, a 10 mm displacement on the transducer could induce up to an average of 19 mV output voltage. While only 0.2 mV is induced with 10 mm transducer displacement with cancellation applied. A 20 dB of SNR improvement was achieved under lab. testing conditions. Figure 4.4 is a sample of circular oriented MGG recording using the plate shaped Hall effect transducer. Trace A is respiratory; Trace B is mucosal MGG and trace C is a reference serosal EGG. The sensing area, about 4 mm wide and 20 mm long, is along the proximal side of the antrum, 50 mm in distance from pylorus. Although strong respiratory interference is still present in trace B, the discernible periodic signal is recognizable if compared with trace C. We assumed that the signal recorded in trace B perhaps is the MGG signal. However, the MGG signal amplitude of about 300 nTesla seems to be much greater than that of magnetic field, 150 pTesla in amplitude, recorded from an isolated frog sciatic nerve[16]. We may start to ask ourself if the signal we measured in this experiment is the true MGG signal.

To confirm our result, we repeated the same test on four different canine subjects. Two recordings showed periodic magnetic signals while other two recordings failed. In the mean time, we managed to confirm this finding in an in-vitro

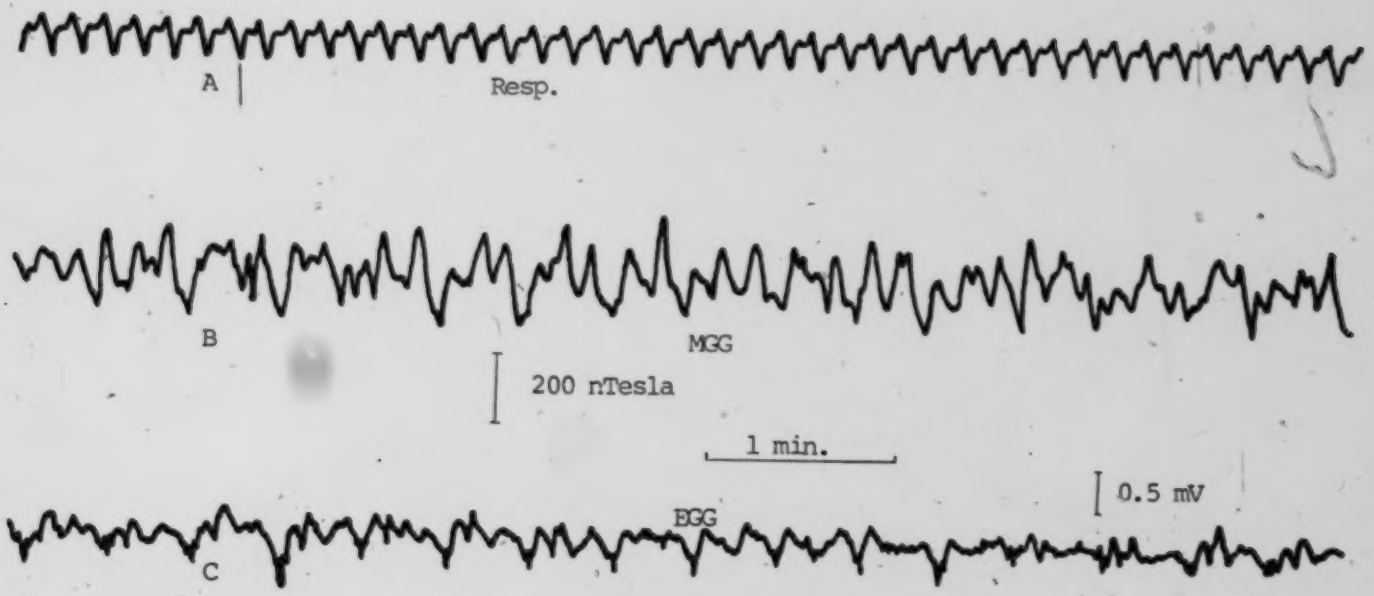

Figure 4.4 A mucosal MGG recording in intact canine stomach

experiment, but the results were not encouraging. We speculate that the antrum under in-vitro condition failed to function normally due to a lack of oxygen. Using an axial Hall effect transducer, we also conducted an experiment to measure MGG in the longitudinal orientation. In this experiment, no discernible MGG signal could be recorded.

4.5 SEROSAL MGG MEASUREMENTS

As stated in our model, the magnetic field can also be measured from the external medium. Using the same recording system as we did for the mucosal MGG measurement, we have positioned the transducer above the surface of the intact antrum. Tests with two transducer orientations were performed, circular and longitudinal respectively. A sample of serosal MGG recording is given in Figure 4.5, where trace A is the respiratory, trace B is serosal MGG and trace C, the serosal EGG. As shown in trace B in Figure 4.5, a MGG signal with better SNR was measured. A one to one relationship of signal periods between MGG and EGG is very obvious. Fourier analysis of trace b and trace c revealed that these two signals

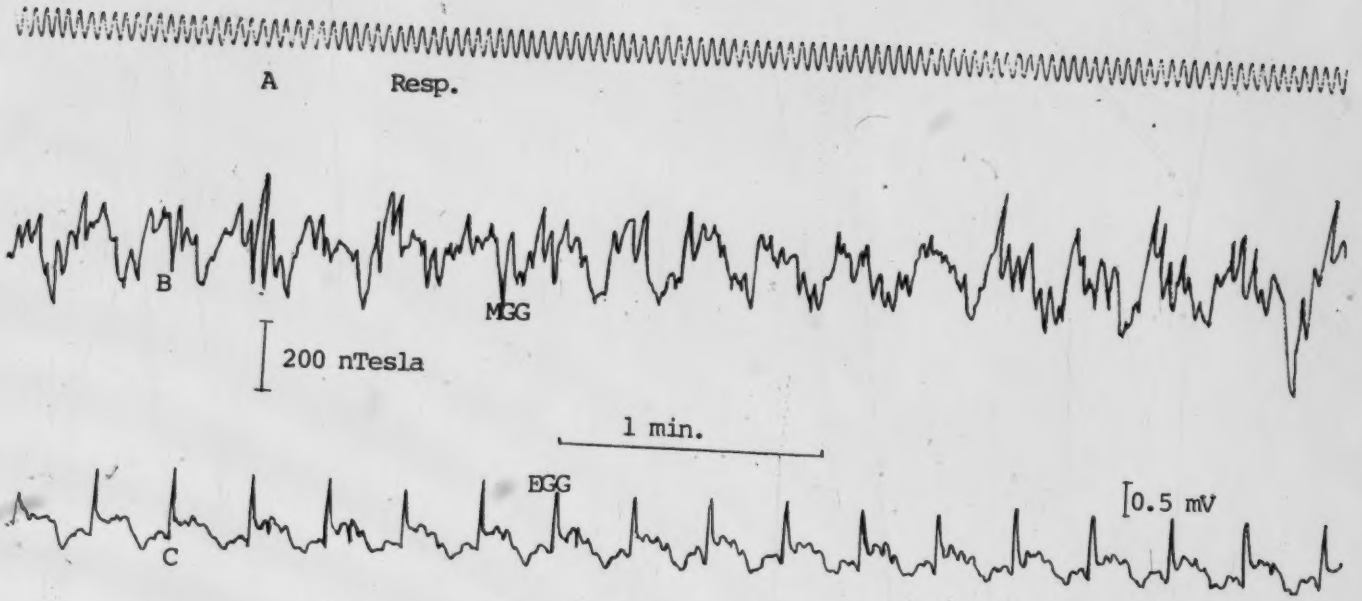

Figure 4.5 A serosal MGG recording in intact canine stomach

have the same frequency components. Figure 4.5a and 4.5b have shown the FFT's of these two signals.

Notice that the muscle displacement can also cause variation of magnetic field. One question immediately arises as the antrum muscle contraction certainly produces a small amount of muscle displacement. A magnetic signal may be induced by this displacement. However, we found that the motion of antrum muscle caused by respiration is about 2 to 4 times greater than that of contractions. Furthermore, examining trace B we found that the MGG signal is about 2 to 3 times greater than that of respiratory artifact. Therefore we tend to come to the conclusion that trace B is the true MGG signal caused by the EGG potential in antrum muscle. However we still can not fully explain why the MGG signal recorded in our experiment is about a thousand times greater than the magnetic field in a nerve fiber.

5.6 DISCUSSION

Mucosal and serosal MGG measurements have shown that the MGG signal traces have the same period as that of EGG's.

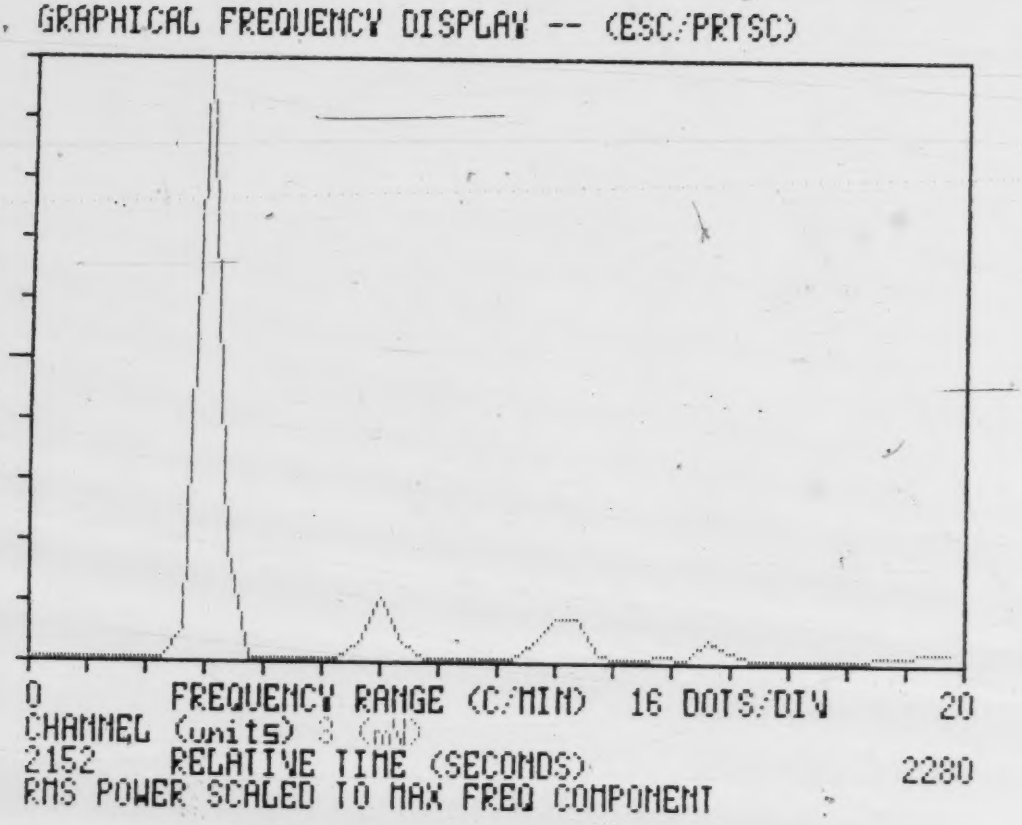

Figure 4.5a FFT of serosal EGG

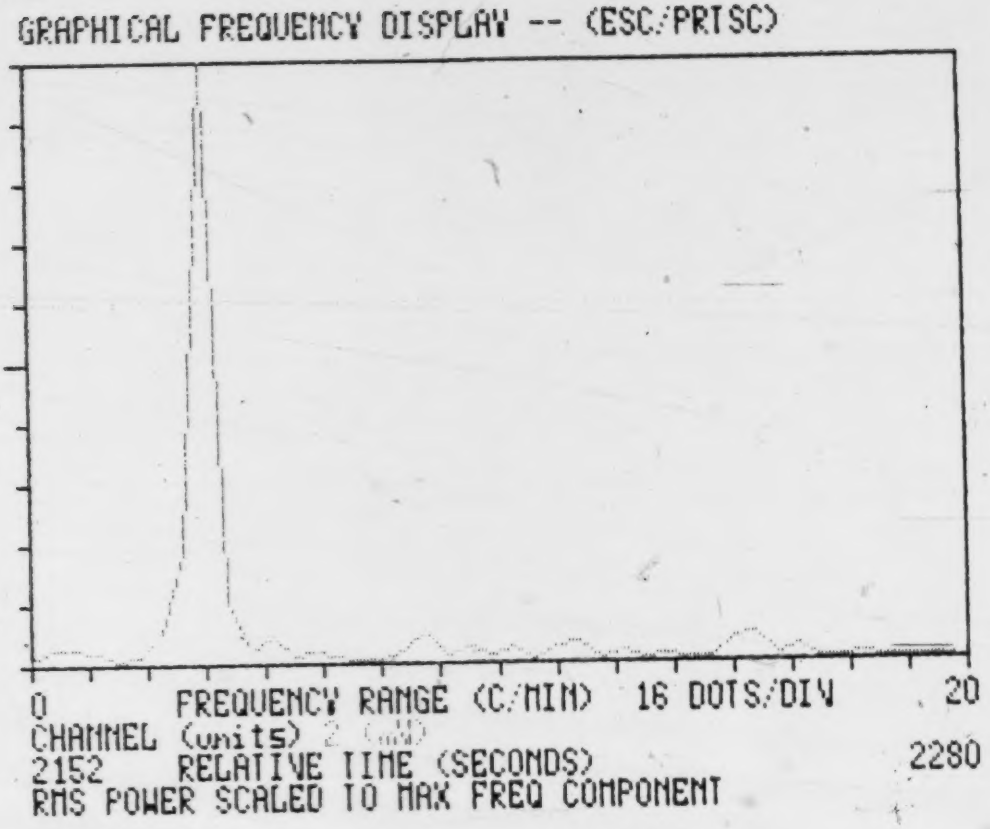

Figure 4.5b FFT of serosal MGG

Secondly, an MGG amplitude of about 300 nTesla is recorded. It is reported that the magnetic field on a single nerve fiber surface can be of the order of 0.1 pTesla in the axial direction. This magnetic field is caused by a single dipole of 70 mV peak to peak potential with 5 to 10 μA axial current[16]. However, in antrum muscle, thousands of dipoles line up to form a dipole band, The longitudinal current, we speculate, would be 2 or 3 orders greater than that of a single dipole nerve fiber. Therefore, the associated magnetic field strength on the surface of antrum muscle could reach the nTesla or tens of nTesla level, which is very close to the MGG amplitude obtained in our experiments.

4.7 SUMMARY OF CHAPTER 4

In this chapter, a mathematical model describing the magnetic field generated from the current source in stomach muscle is introduced. In this model, we assume that only the axial current exists and the resultant magnetic fields relate only to this current. A Gaussmeter was used to measure the gastric magnetic fields in canine stomach. The recordings have shown the periOdic magnetic signals. However, we still cannot confirm whether it is the true MGG. More precise experiments

need to be done to examine the magnetic fields in the stomach.

Next chapter will discuss a method that was used to measure the gastric contractile activity.

Chapter 5

MEASUREMENT OF CONTRACTILE ACTIVITIES IN STOMACH

5.1 INTRODUCTION

One of the important aspects of gastric motility is gastric contractile activity. In 1914, Alvarez investigated gastrointestinal contractions[1], and later, he studied the link between gastric contractile activity and electrical activity in the stomach[2]. It is shown in Alvarez's work that the mechanical activity occurs in stomach as distaly moving peristaltic contraction waves and powerful antral contractions; gastric mixing and emptying are the consequences of gastric electrical activities which were later defined by other researchers as Electrical Control Activity (ECA); or Basic Electrical Rhythm (BER), slow wave, and Electrical Response Activity (ERA) [4-7]. The gastric ERA which is responsible for gastric contractile activities is usually described as spike potentials and the increase of the second components in action potentials[4-6]. The mechanism

of the ERA is quite complex. However, it is reported that the contractions in gastrointestinal smooth muscle are caused by a large increase of calcium influx through the cell membrane [5,8], and careful experiments have shown that hormonal and nervous control of gastric motility perform a key role [4,9].

The measurements of gastric contractile activity perhaps are the earliest experiments performed on stomach[1], and there are several methods and techniques that are applicable from a clinical point of view[6,7,16]. The most common methods applied in the diagnosis are multisite perfusion, sutured strain gauge, and radiographic methods. These diagnostic techniques are performed separately and usually do not acquire simultaneous gastric electrical recording for comparison. The close relationship between gastric EGG and contractile activities indicates that the methods which provide simultaneous recording of gastric EGG and contractions are valuable.

In this chapter, we will introduce a method which can be used successfully to measure simultaneous gastric contractile activity and gastric electrical activity in humans and animals.

5.2 GASTRIC CONTRACTILE MEASUREMENT USING THE BALLOON ELECTRODE ASSEMBLY

This method using an assembly of electrodes mounted on a balloon differs from the multisite perfussion technique in that it measures the contractile activity of the whole antrum but with higher sensitivity. Also, it differs from the methods that use sutured strain gauges or radioactive substances. The balloon contraction measurement is not invasive like the sutured strain gauges nor does it have a radioactive impact on the body. As shown in Figure 5.1, the balloon electrode assembly is placed in the terminal antrum under fluoroscopy. The typical length of the balloon is about 8 cm. One air channel in the nasal tube is open to the balloon, and then connected to a pressure gauge. The pressure gauge is calibrated to provide a sensitivity of 0.1 volts per cm H_2O. The output voltage signal of the gastric pressure sensor is fed into a preamplifier, followed by appropriate filters, and finally, stored in the computer for off-line analysis. As mentioned before, the pressure balloon registers the total pressure changes in the antrum.

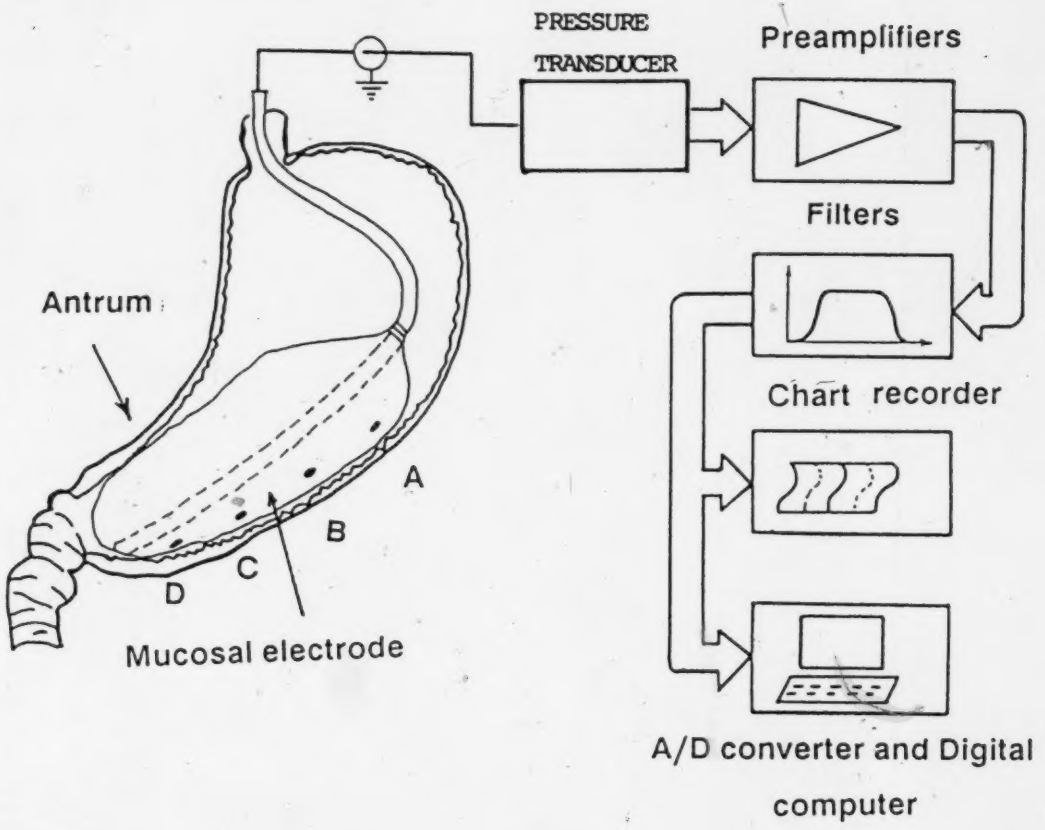

Figure 5.1 A schematic diagram of gastric intraluminal pressure measurement system

In normal human terminal antrum, due to its size, only a single contractile wave front can be registered by the pressure balloon.

A typical recording of simultaneous mucosal EGG and stomach contractile activity in anesthesized canine stomach is given in Figure 5.2.

In Figure 5.2, trace A is respiration, trace B, C and D are the mucosal EGG's, and trace E is gastric contraction activity. By inspecting the mucosal EGG recording we found that:

a) the ECA is propagating distally from mid copus to the terminal antrum,

b) the gastric contraction waves which show peak to peak amplitudes of 3.5 to 4 cm H_2O per division, and they are accompanied by gastric ECA cycles,

c) in this recording, only small peristaltic contractions are shown; no powerful gastric contractions were registered in this particular experiment. Perhaps very deep general anesthesia affects the normal canine MIC cycles and partially abolishes strong gastric contractions.

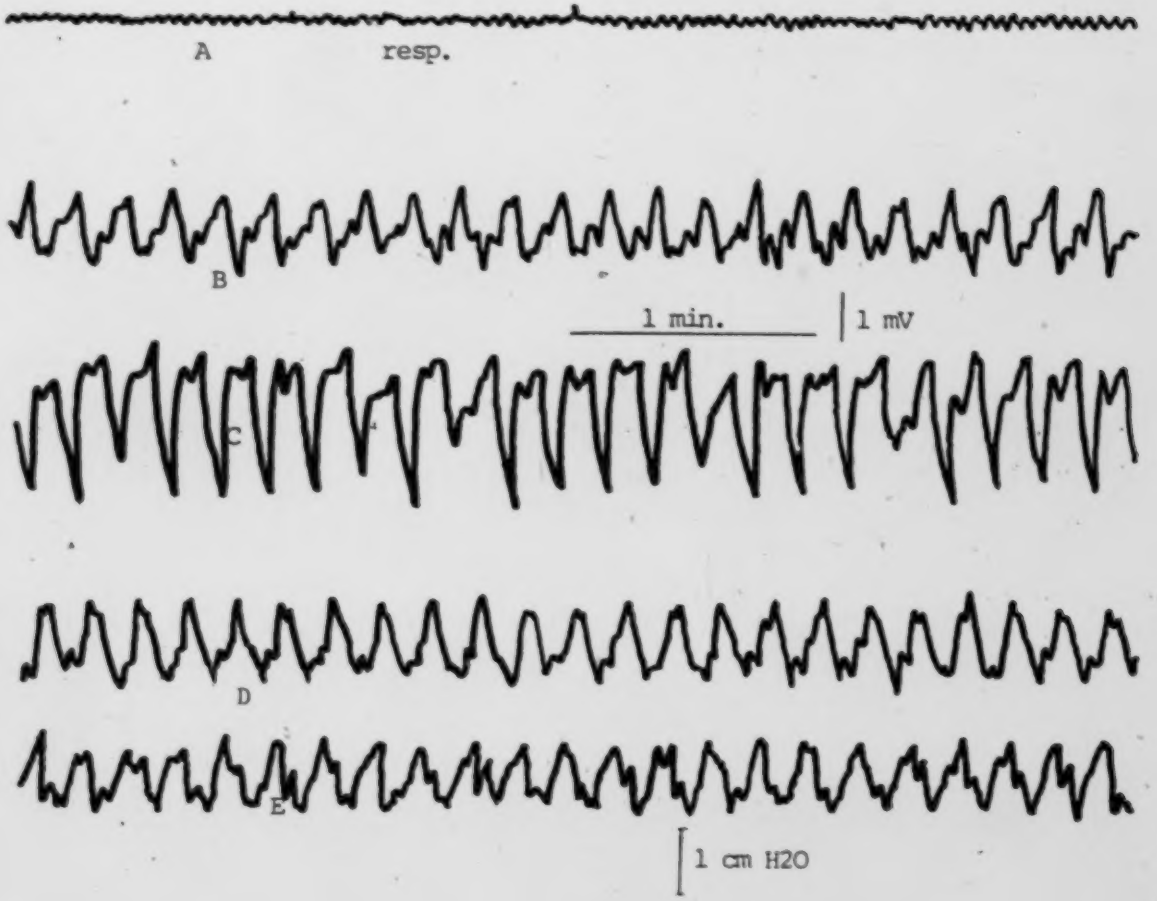

Figure 5.2 Simultaneous measurement of gastric mucosal EGG and gastric intraluminal pressure in canine stomach

We have already shown, in Figure 3.12, that powerful gastric contractions can be clearly measured in canine stomach if they occur. In Figure 3.12, one of the powerful contractile waves occurred and it showed superimposed small periodic contractile waves. Also the gastric mucosal EGG was temporarily disturbed as can be seen in Figure 3.12 Successful applications of gastric pressure measurement were performed in conscious human subjects. Figure 5.3 is a sample of human simultaneous mucosal EGG and gastric contractile activity. In Figure 5.3, trace A, B, C and D are mucosal EGG signals. Trace E is gastric contractile activity in antrum and trace F is the respiration. As we can see from Figure 5.3:

a) the distal propagation of ECA waves is obvious from trace A to D and,

b) it is very clear that the antrum contractile waves accompany each ECA cycle with an amplitude of 4 to 12 cm H_2O per division and,

c) in trace E, the gastric contractile waves are approximately in phase with ECA's, which indicate that a series of relative strong gastric peristaltic contractions is prevailing in the terminal antrum and,

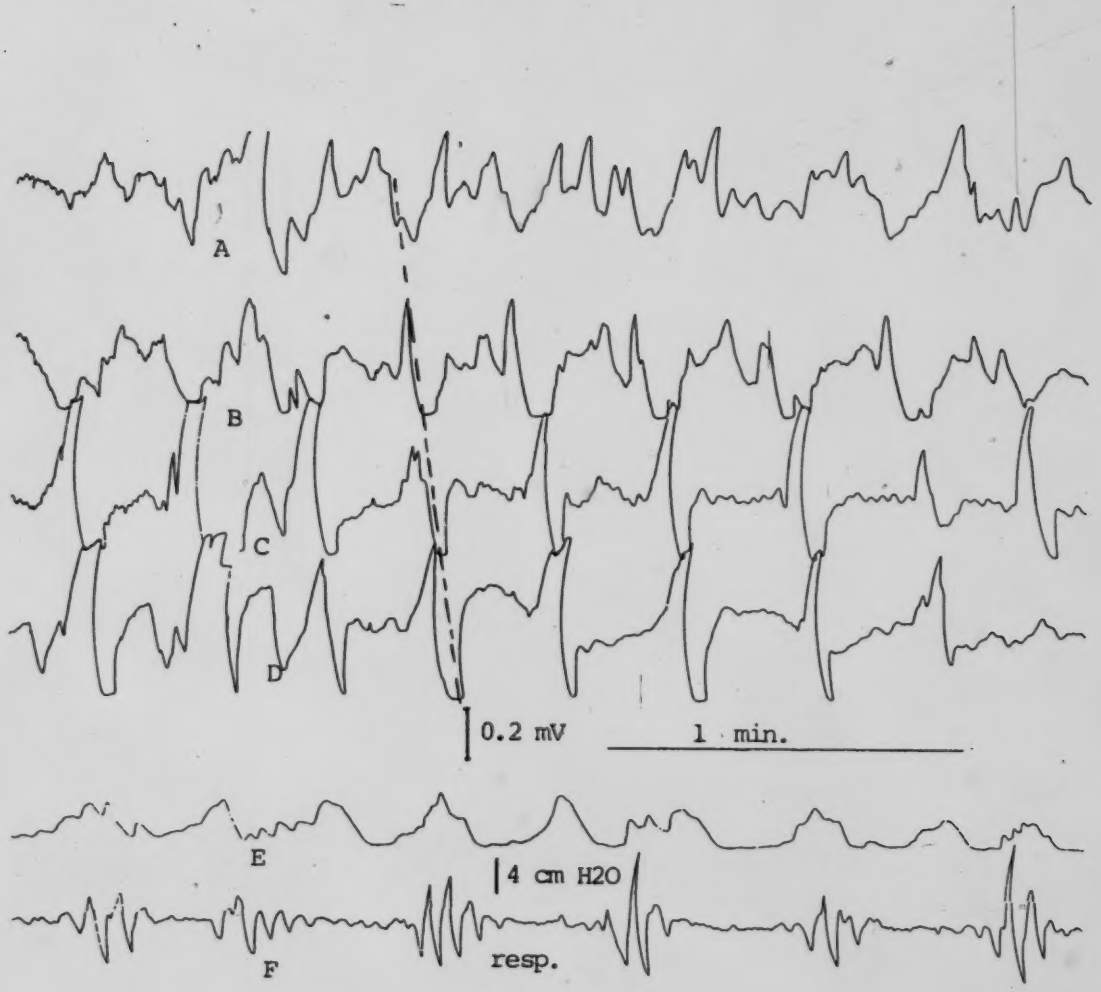

Figure 5.3 A recording of human EGG, gastric intraluminal pressure and respiration. It is shown that the trace E has the same frequency as that of EGG's

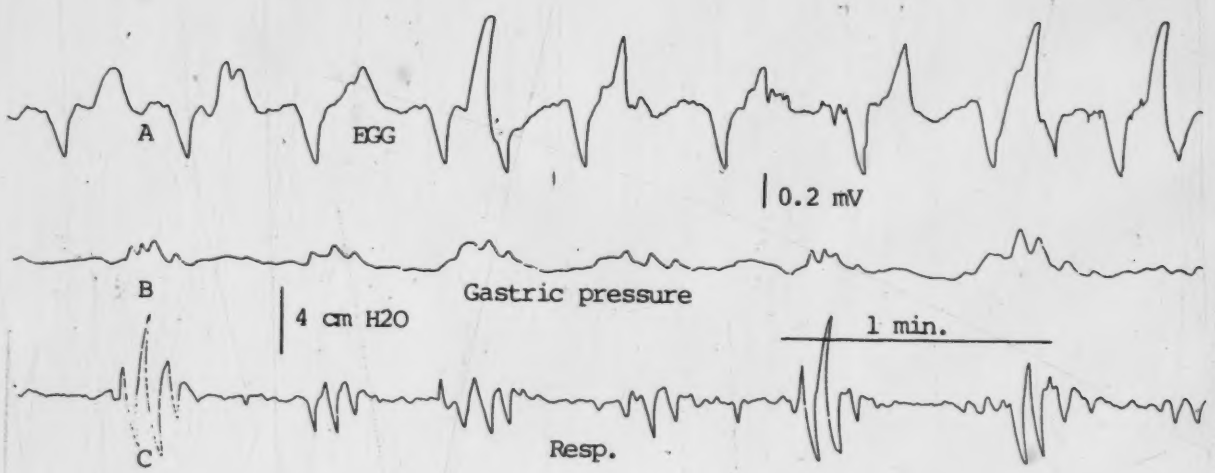

Figure 5.4 A recording of human mucosal EGG, gastric intraluminal pressure and respiration. It is shown that gastric contraction occurs at a lower frequency than that of EGG's

d) abnormal respiration signal patterns are probably due to the improper transducer position on the chest.

Figure 5.4 is a human EGG and gastric intraluminal recording that shows lower gastric contractile frequency than that of mucosal EGG's.

5.3 SUMMARY OF CHAPTER 5

In this chapter, a method to measure gastric contractile activity is introduced. Using a balloon to measure gastric pressure changes was shown to be a sensitive, simple and non-invasive method that can be applied in human gastric intraluminal pressure measurements. Generally, during the test, the stomach muscle is maintained in a nonstretched state which is appreciated for measuring spontaneous gastrice contractions. Although the gastric contractions can be easily measured using the pressure balloon, mucosal EGG's are sometimes disturbed by strong distal antrum contractions, and the gastric contraction measured may represent the sum of multiple contractile waves if two ECA potentials occur in the length of pressure balloon. So far, this appears to be the only

type of gastric EGG assembly, which provides four channels of mucosal EGG signals and simultaneous gastric intraluminal pressure signals.

CHAPTER 6 OVERALL SUMMARY AND CONCLUSIONS

In this study, a brief historical background of measurements of gastroelectrogram has been given and the current mucosal EGG recording methods have been examined, as well, several new types of mucosal EGG measurement techniques have been developed. The advantages and disadvantages of those methods were discussed. The recording using the balloon electrode assembly on canine stomach in in-vivo mucosal EGG measurements under anesthetization has shown that the temporal and spatial organizations of EGG can be correctly obtained. Human mucosal EGG measurements using the balloon electrode assembly have not been fully successful; the reasons are given in chapter 3.

A technique of using stainless steel clips to record mucosal EGG has been developed and tested on canine stomach, and human experiment using clip electrodes has been designed.

In chapter 4, A mathematical model was developed to study the gastric magnetic fields. We assume that there are magnetic fields associated with gastric electrical activities in

stomach. The magnetogastrogram (MGG) can be measured on the surface of the stomach wall. To support our model, attempts to measure MGG have been made using a Gaussmeter. Preliminary results are given. Some limits on MGG measurement were also discussed.

In chapter 5, a method to measure simultaneous gastric contractile activities while measuring gastric electrical activities was given. A pressure gauge was used to record the pressure change in the balloon. Human and animal experiments have shown that both weak and strong gastric contraction in antrum can be registered.

This study has provided a handful of experimental results on mucosal electrical activity measurements and a number of methods for the design of gastric electrode assemblies. These will be certainly helpful for the further studies on EGG measurements.

MGG can be predicted using the model introduced in this study. Right now we still do not have enough evidence to confirm our MGG recordings and more experiments will be needed

in the future studies.

REFERENCES:

1] Alvarez,W.C . FUNCTIONAL VARIATIONS IN CONTRACTIONS OF DIFFERENT PARTS OF THE SMALL INTESTINE. Am. J. Physiol. 1914, 35:177-193.

2] Alvarez, W.C. and Mahoney, L.J. ACTION CURRENT IN STOMACH AND INTESTINE. 1922, Am. J. Physiol. 58:476-493.

3] Alvarez, W.C. THE ELECTROGASTROGRAM AND WHAT IS SHOWS. J. Am. Med. Asso. 1922, 78:1116-1119.

4] Code, C.F, Szurszewski, J. H.,Kelly, K.A.and Smith,I.B. A CONCEPT OF CONTROL OF GASTROINTESTINAL MOTILITY. HANDBOOK OF PHYSIOLOGY, Edited by C. F. Code. pp 2881-2896 .1968.

5] Kelly, K. A. Code, C.F.and Elvebach,L.R. PATTERNS OF CANINE GASTRIC ELECTRIC ACTIVITY. Am.J. Physiol. 1969,217:461-470.

6] Sarna,S.K., Daniel, E.E. and Kingma, Y.J. SIMULATION OF THE ELECTRICAL CONTROL ACTIVITY OF THE STOMACH BY AN ARRAY OF RELAXATION OSCILLATORS. Am. J. Dig. Dis. 1972, 17:299-300.

7] Smout,A.M, E.J. Vander Schee, and J.L. Grashuis. WHAT IS MEASURED IN ELECTROGASTROGARPHY? Dig. Dis and Sci. 1980, 25:No3 179-187.

8] Joseph H. Szurszewski, ELECTRICAL BASIS FOR GASTROINTESTINAL MOTILITY . Physiology of the Gastrointestinal Tract. Edited by Leonard R. Johnson. Raven Press. 1981, 1435-1466

9] Keith A. Kelly, MOTILITY OF THE STOMACH AND GASTRODUODENAL JUNCION, Physiology of the Gastrointestinal Tract, Chapter 12, Edited by Leonard R. Johnson. Raven Press, New York, 1981.393-409.

10] Sarna, S.K. and Daniel, E.E. THRESHOLD CURVES AND REFRACTORINESS PROPERTIES OF GASTRIC RELAZATION OSCILLATORS. Am. J. Physiol. 1974, 226:749-755.

11] Sarna, S.K. and Daniel, E.E. ELECTRICAL STIMULATION OF GASTRIC ELECTRICAL CONTROL ACTIVITY. Am. J. Physiol. 1973, 225:125-131.

12] Dalu. Peng, Kingma,Y.J. and Bowes, K.L. DESIGN OF A SELFADHERING GASTRIC MULTICHANNEL ELECTRODE ASSEMBLY. IEEE BME, 9th Annual Conference in Boston, Nov, 1987

13] Kingma, Y.J., Durdle, N.G, Lenhart, K. and Bowes, K. L. IMPROVED AG/AGCL PRESSURE ELECTRODE. Med. and Biol. and Comp. 1978, 21:351-357.

14] John W. Hamilton, Bader, E, Bellahsene, Mark Reichelderfer, J. G. Webester and Paul Bass. HUMAN ELECTROGASTROGRAMS: COMPARISON OF SURFACE AND MUCOSAL RECORDINGS. Dig. Dis and Sci. 1986.31:

15] Stoddard, C.J. Smallwood, R.H. and Duthie, H.L. ELECTRICAL ARRHYTHMIAS IN HUMAN STOMACH. Gut, 1981, 22:705-721.

16] Chul H. You, and William Y. Chey, STUDY OF ELECTROMECHANICAL ACTIVITY OF THE STOMACH IN HUMANS AND IN DOGS WITH PARTICULAR ATTENTION TO TACHYGASTRIA. Gastroenterology. 1984 . 86:1460-1468.

17] N.Mirizzi, R. Stella and U. Scafoglieri. MODEL TO SIMULTE THE GASTRIC ELECTRICAL CONTROL AND RESPONSE ACTIVITY ON THE STOMACH WALL AND ON THE ABDOMINAL SURFACE. Med. Biol. Eng. and

Comp. 1986. 157-163.

18] Mirizzi, N. and Scafoglieri, U. OPTIMAL DIRECTION OF ELECTROGASTROGRAPHIC SIGNAL IN MAN. Med. Biol. Eng. and Comp.1983.21: 385-389.

19] Mirizzi, N, Stella, R and Scafoglieri, U . A MODEL OF EXTRACELLULAR WAVESHAPE OF THE GASTRIC ELECTRICAL ACTIVITY. 1985. Ibid.,23:33-37.

20] John, C and R.Plonsey. A MATHEMATICAL EVALUATION OF THE CORE CONDUCTOR MODEL. 1966, biophsical J. 6:95-112.

21] John, C and R. Plonsey. THE EXTRACELLULAR POTENTIAL FIELD OF THE SINGLE ACTIVE NERVE FIBERIN A VOLUME CONDUCTOR. Biophysical J. 8:842-864. 1968.

22] R. Plonsey and R.C.Barr. CURRENT FLOW PATTERNS IN TWO-DIMENSIONAL ANISOTROPIC BISHNCYTIA WITH NORMAL AND EXTREME CONDUCTIVITIES. Biophysical J. 1984. 45:557-571.

23] Plonsey,R. VOLUME CONDUCTOR FIELDS OF ACTION CURRENTS.

Biophysical J. 1964.4:318-328

24] Geselowitz, C. B. COMMENT ON THE CORE CONDUCTOR MODEL. Biophysical J. 1966, 6:691-692

25] Barr, R.C. and Plonsey, R. PROPAGATION OF EXCITATION IN IDEALIZED NONISOTROPIC TWO-DIMENSIONAL TISSUE. Biophysical J. 1984. 45:1191-1220

26] Woosley, J.K, Roth,B J. and Wikswo J.P. THE MAGNETIC FIELD OF A SINGLE AXON: A VOLUME CONDUCTOR MODEL. Math. Biosci.1985.76:1-36.

27] John Paul Barach, Bradley J. Roth, and H. P. Wikswo. MAGNETIC MEASUREMENTS OF ACTION CURRENTS IN A SINGLE NERVE AXON: A CORE CONDUCTOR MODEL. 1985. IEEE BME 32:2, 136-140.

28] Bradley J. Roth and John p. Wikswo, JR. THE ELECTRICAL POTENTIAL AND THE MEGNETIC FIELD OF AN AXON IN A NERVE BONDLE. 1985, Math. Biosci.76:37-57.

29] Bradley J. Roth and J. P. Wikswo, JR. A BIDOMAIN MODEL FOR THE EXTRACELLULAR POTENTIAL AND MEGNETIC FIELD OF CARDIAC

TISSUE. IEEE BME 33:4 467-469.

30] John P Wikswo,JR. MAGNETIC FIELD OF A NERVE IMPULSE: FIRST MEASUREMENTS. Scince208:53-55.

31] John P. Wikswo, JR., Philip C. Samson and Robin P Giffard. A LOW NOISE LOW INPUT IMPEDANCE AMPLIFIER FOR MAGNETIC MEASUREMENTS OF NERVE ACTION CURRENTS. IEEE BME30. 4:215-221.

32] Familoni. B.B. NONINVASIVE ASSESSMENT OF GASTRIC MOTILITY. An Ph,D thesis of the Department of Electrical Engineering, University of Alberta, Canada, 1986.

33] G. Mclanchlan, N. M. M. Buchanam, G. P/ Crean and K. E. L. McColl. AN ENDOSCOPIC PROCEDURE FOR ACCURATE LOCALISATION OF INTRALUMINAL PH ELECTRODES Endoscopy. 19 (1987) 124-126.